

**Coherence Analysis of an “X”-shaped Aperture using Piecewise  
Diffraction**

by

**David Andrew-Stephen Hill**

---

Copyright © David Andrew-Stephen Hill 2016

A Thesis Submitted to the Faculty of the  
DEPARTMENT OF OPTICAL SCIENCES

In Partial Fulfillment of the Requirements  
For the Degree of

MASTER OF SCIENCE

In the Graduate College

THE UNIVERSITY OF ARIZONA

## STATEMENT BY AUTHOR

### STATEMENT BY AUTHOR

This thesis has been submitted in partial fulfillment of requirements for an advanced degree at the University of Arizona and is deposited in the University Library to be made available to borrowers under rules of the Library.

Brief quotations from this thesis are allowable without special permission, provided that accurate acknowledgment of source is made. Requests for permission for extended quotation from or reproduction of this manuscript in whole or in part may be granted by the copyright holder.

SIGNED: \_\_\_\_\_

### APPROVAL BY THESIS DIRECTOR

This thesis has been approved on the date shown below:

\_\_\_\_\_

Tom D. Milster

Professor of Optics

\_\_\_\_\_

Date

## **ACKNOWLEDGEMENTS**

There are many people who have helped me throughout the development of this thesis to whom I am grateful. I would like to thank Tom Milster who has been a great mentor and inspiration during my time at the University of Arizona. Without his support this project never could have succeeded. Finally, I would like to dedicate this work to my mother especially and my entire family for their unconditional support.

## TABLE OF CONTENTS

Table of Contents.....	3
List of Figures.....	5
List of Tables.....	8
Abstract.....	7
Chapter 1: Introduction.....	8
Chapter 2: History.....	10
Chapter 3: Background.....	12
Chapter 4: Theory.....	19
Setup.....	19
Results.....	25
Chapter 5: Experimentation.....	27
Setup.....	27

Spatial Coherence Visibility Factor.....	27
Conclusions.....	28
References.....	29

## LIST OF FIGURES

Figure 1 Division of wavefront Interferometer.....	10
Figure 2 YDSI Pinhole Pairs.....	11
Figure 3 Michelson Interferometer.....	14
Figure 4 Young's Double Pinhole Interferometer.....	18
Figure 5 Irradiance Profile, Visibility vs. OPD.....	19
Figure 6 Projection Vector $\mathbf{d}$ .....	21
Figure 7 X-Aperture and Different Pinhole Spacing.....	23
Figure 8 Family of Hyperbolas.....	24
Figure 9 Piecewise X-Aperture Model.....	25
Figure 10 Flow Chart of Simulation .....	26
Figure 11 Diffraction & Interference Irradiance Pattern.....	30
Figure 12 Optical Design.....	31
Figure 13 Family of Hyperbolas Simulated.....	32
Figure 14 Flow Chart of Fitting Routine.....	33
Figure 15 Irradiance Profile Showing Column Vectors.....	35
Figure 16 Visibility vs PH separation.....	36
Figure 17 Edge Diffraction .....	37
Figure 18 Illustration of an X-Aperture with Center Block.....	42
Figure 19 Image of X-Aperture.....	43

Figure 20 X-Aperture Setup.....	45
Figure 21 Gray-scale Image with X-Y Axis.....	48
Figure 22 Results of Poorest Fit.....	49
Figure 23 Results of Best Fit.....	50
Figure 24 SEM Image of Slit Width.....	52
Figure 25 SEM Image of Angle Measurement for 10 $\mu$ m Slit Width.....	53
Figure 26 SEM Image of Angle Measurement for 12 $\mu$ m Slit Width.....	53
Figure 27 SEM Image of X-Aperture with Center Block.....	54

## LIST OF TABLES

Table 1 Design Parameters.....	27
Table 2 Source Diameter Error.....	28
Table 3 X-Apertures.....	42
Table 4 Circular Apertures.....	44
Table 5 Fit Results of Source Diameter.....	51



## ABSTRACT

The motivation of the experiment is to accurately determine the spatial coherence of a 370nm ultraviolet light emitting diode using one single interferogram. We report a novel method of measuring the spatial coherence of a 370nm UV LED source without using complicated optics. This is done by fabricating an aperture similar to a Young's Double Slit Interferometer (YDSI) on the Maskless Lithography Tool (MLT). The aperture contains two slits in an otherwise opaque aperture that has the two slits at an angle  $\theta_{ap} = 21.6^\circ$  relative to one another in the shape of an "x" where the slit length is 2mm long. A simulation of the experiment is performed using theory called piecewise diffraction theory in a Matlab© package called OptiScan. Piecewise diffraction is the approximation of a surface as a collection of infinitesimal windows. When the light field is incident upon each window, piece-by-piece, there is a corresponding diffracted pattern in the observation plane. The piecewise diffracted field within the simulation yields an interferogram in the shape of a family of hyperbolas in the observation plane. The interferogram is loaded into the Matlab script to calculate the visibility and fit that to an effective source size. The source size is the figure of merit for the integrity behind the piecewise diffraction theory. In the experiment, the x-shaped aperture is placed 2cm from the camera array, while the source is fixed 1m from the x-aperture. This interference pattern is input to a Matlab© script that fits the size of the source to the measured spatial

coherence visibility factor. In the fit routine, each column in the image is scanned for a minimum and maximum irradiance value to calculate visibility and fit that value to an effective source size. The results for a 10 $\mu$ m slit width x aperture from the simulation yield a 1.40mm source diameter for an actual source size of 1.5mm. The results from the experiment showed a 1.40mm source diameter for a 16 $\mu$ m slit width with an opaque (block) center of the aperture and 1.45mm source diameter for a 14 $\mu$ m slit width. In future work the x-aperture geometry should be fabricated with values closer to the modeled. Also, the dramatic effect of the temporal coherence should be subtracted as a factor to the calculation of visibility.

## CHAPTER 1: INTRODUCTION

Spatial coherence is defined as the dependence of the correlation between two points in a light field due to the source size and shape. By measuring the degree of coherence, the spatial extent of a quasi-monochromatic incoherent extended source can be estimated. In this study, we present a method to measure the spatial coherence visibility factor, which is related to the mutual intensity, from an interferogram produced by an x-shaped aperture. This information is used to extract the effective source size.

The method of measuring the spatial extent of a source in this way presents a simple method to determine coherence properties of a source. It is inexpensive and robust in design, making it a preferable alternative to techniques using multiple measurements. To date, the methods described in this thesis have fewer optical components in the measurement system, with only one stationary aperture, compared to similar measurement systems that have been reported. In essence, the optical system is a collection of multiple double pinhole interferometers with different pinhole distances combined into one aperture.

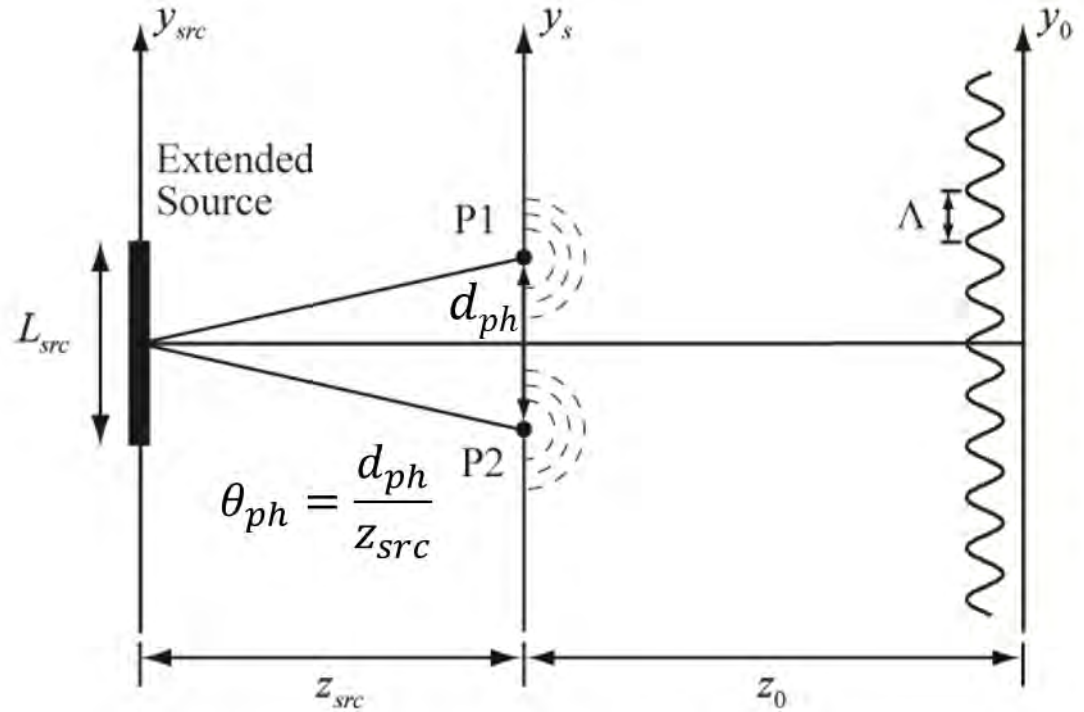
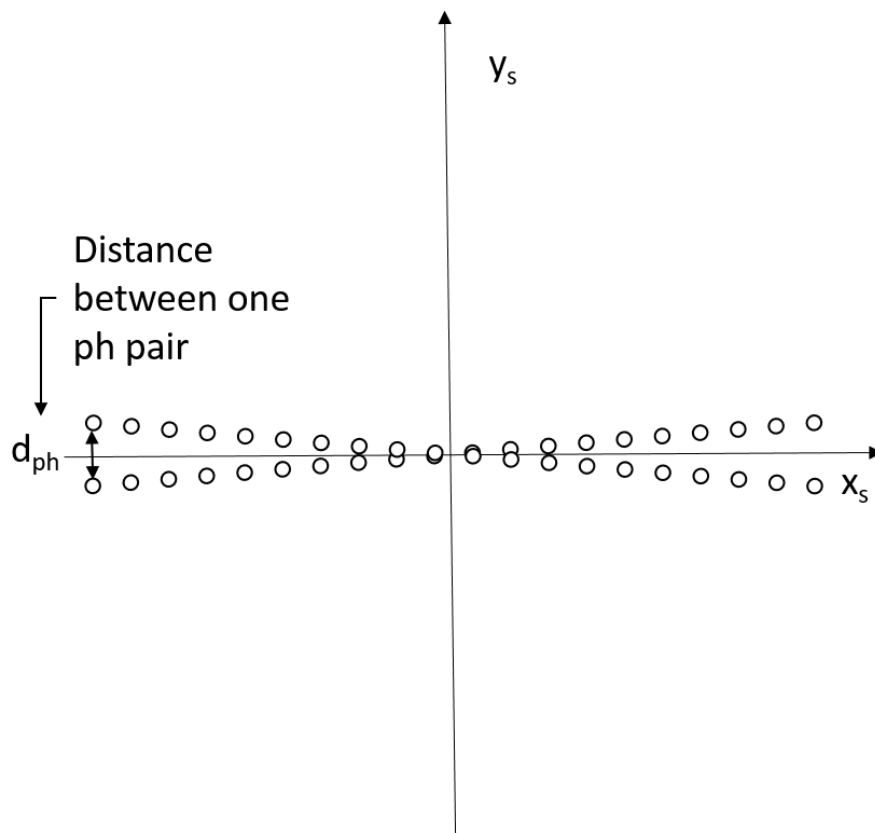


Figure 1: One dimensional source distribution with length  $L$  and angular subtense  $\theta$ . [1]

Figure 1 illustrates a simple division-of-wavefront Young's double pinhole interferometer (YDPI) setup resembling the concept behind the experiment in this thesis. Each point on an extended, quasimonochromatic, incoherent line source with a wavelength  $\lambda$  produces a spherical wavefront that propagates to the aperture. The aperture samples the wavefront at two different points in space P1 and P2 separated by distance  $d_{ph}$  along the  $y$ -dimension. The wavefront is transmitted through the pinholes and the two resulting diffracted wavefronts interfere with one another to produce a fringe pattern in the observation plane.

The visibility for the example in Figure 1 is a function of the length of the line source  $L_{src}$ . Decreasing  $L_{src}$  decreases the maximum fringe shift and therefore increases visibility. The angular subtense  $\theta_{ap}$  is the ratio between  $d_{ph}$  and  $z_{src}$ . If this parameter is decreased by way of increasing the distance  $z_{src}$  to the source from aperture, then fringe visibility also increased. [1]

The x-aperture design is closely related to a YDPI and is modeled as a collection of tiny pinhole pairs with diameters on the order of microns. Figure 2 below illustrates the modeling concept that is discussed in more detail in Chapter 4.



*Figure 2: X-aperture is modeled as a collection of tiny pinhole pairs.*

The x-aperture interferometer is unique, because it contains no moving or expensive parts. Yet, in one measurement, it can determine the spatial coherence characteristics of the source. The aperture is designed in such a way that slits of the “x” induce many different pinhole distances in the x-direction. Diffraction from the slits in the x-aperture is conceptually due to a collection of small holes within the slits. The diffracted fields from the light holes are added linearly to create a modulated fringe pattern at the observation plane. In this work, a piece-wise diffraction algorithm is used to calculate the light pattern on the camera that results from the x-aperture.

Chapter 2 discusses the history behind interference and its relation to spatial coherence. Chapter 3 discusses relevant background information to support the reader’s understanding of interferometry and spatial coherence, including examples of interferometers. Chapter 4 is the theory behind the experiment, and detailed explanation of the experimentation is discussed in Chapter 5. Conclusion for this thesis are presented in Chapter 6.

## CHAPTER 2: HISTORY

In 1664, Robert Hooke, who was a British scientist, introduced the wave theory of light to the world.[2] A decade later, Robert Boyle, the British chemist, expanded Hooke's idea of the wave theory of light. Based on these ideas, Christiaan Huygens published a report entitled, *Treatise of Light*,[3] which explained that light waves were an aggregate of tiny wavelets that are now referred to as Huygens wavelets. Around the same time, Isaac Newton focused on the contrasting idea that light was a particle comprised of associated wavelengths, and in 1666 Newton observed the spectrum of white light from the refraction of the light through a prism. Newton and Hooke rivaled one another, due to their ideas about the science behind light.

Thomas Young, an English physician, focused much of his research on the physiological aspect of the human eye as it relates to light and color.[4] In 1793, he explained how the curvature of the crystalline eye lens contracts and expands, changing the power of the eye to accommodate human vision. Other accomplishments of Young were the affirmation of the human eye's response to three primary colors and the phenomenon of astigmatism in the eye. The most notable work, which is of special importance to the experiment described within this paper, is Young's double-slit experiment.[4] In order to verify and prove his wave theory of light, he placed a card with a nominal width of  $\frac{1}{30}$  of an inch in front of a tiny hole in a window to demonstrate the interference of light. Separation of light from the pinhole into two parts created fringes

when the card was inserted, and the fringes disappeared when the card was removed. The wave theory was then expanded to include polarized light with a glass rhombus by Augustin-Jean Fresnel.[5] Fresnel was also responsible for the famous equations that govern reflection and refraction of light based on differing refractive indices within two separate media.

Young's double slit experiment implied another physical phenomena that we now know as diffraction. Fresnel derived the expressions describing diffraction of monochromatic electromagnetic fields propagating from an aperture. Gustav Kirchoff, the German physicist, used Green's theorem and James Clerk Maxwell's electromagnetic equations to derive the expression for what is now known as the Kirchoff-Fresnel diffraction formula.[6] Scientists use this diffraction and similar formula to solve for diffraction patterns in the Fresnel region, *i.e.* close to the aperture. The linearity of these diffraction formulas assists in the description of the superposition of sufficiently small piecewise-constant elements discussed in Chapter 4 of this manuscript.



Young's development of the world's first light-wave interferometer pioneered the study of interferometry, which is the study of interfering light waves. Interferometers have been used extensively in radio astronomy and microscopy. For example, there is an ongoing project in South Africa building the Square Kilometer Array (SKA) radio telescope that will eventually become the world's largest telescope.[7] Its baseline stretches from the northern parts of South Africa to Australia. Another interferometer is the Michelson Stellar Interferometer discovered by Albert Michelson in 1893.[8] This type of interferometer samples the wavefront from the light source with two mirrors and folds the light path with two other mirrors, as shown in Figure 3. A Michelson Stellar Interferometer measures the angular separation of binary star systems, and information about the stars' spatial characteristics can be extracted from such data. This interferometer, built on Mount Wilson in 1920, was used to measure the diameter of the star Betelgeuse. [9] The fringe visibility is measured as a function of  $h$  with multiple measurements, and the star's angular extent is calculated from these data. The Michelson interferometer is conceptually similar to the x-aperture technique, except data for all separations are collected in a single x-aperture measurement.

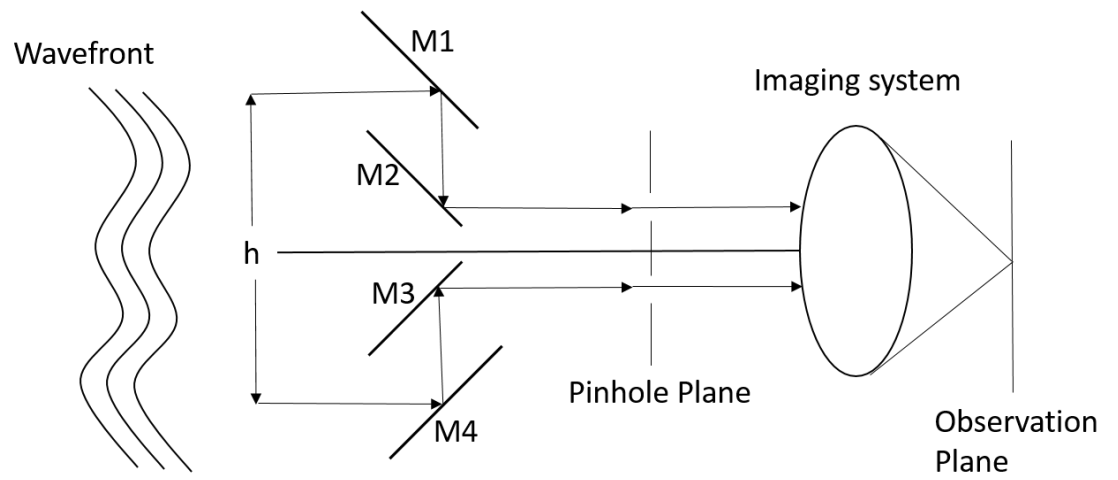


*Figure 3: Michelson Stellar Interferometer.*

### CHAPTER 3: BACKGROUND

Suppose two equal-amplitude plane waves propagate along directions  $\widehat{\mathbf{k}}_1$  and  $\widehat{\mathbf{k}}_2$  described by

$$U_1(\mathbf{r},t)=A\exp[j(\mathbf{k}_1\cdot\mathbf{r}-\omega t+\phi_1)] \quad (1)$$

and

$$U_2(\mathbf{r},t)=A\exp[j(\mathbf{k}_2\cdot\mathbf{r}-\omega t+\phi_2)], \quad (2)$$

where  $\mathbf{k}_1 = \frac{2\pi}{\lambda}\widehat{\mathbf{k}}_1$  and  $\mathbf{k}_2 = \frac{2\pi}{\lambda}\widehat{\mathbf{k}}_2$ ,  $\mathbf{r}$  is the position vector, the  $(\cdot)$  is dot product,  $\omega$  is the radian frequency of light and  $\phi$  is offset phase. If the medium is linear, the principle of superposition applies, and the waves combine by simply adding the two fields. Each wave has a real part and an imaginary part, and the real field of the wave is represented as

$$\text{Re}\{U_1(\mathbf{r},t)\}=A \cos(\mathbf{k}_1\cdot\mathbf{r}-\omega t-\phi_1) . \quad (3)$$

Exploiting a known identity,  $\cos(A)+\cos(B)=2 \cos[(A+B)/2]\cos[(A-B)/2]$ , the real electric field of the combination is written as

$$\text{Re}\{U(\mathbf{r},t)\}= 2A\cos[1/2 (\mathbf{k}_\Delta\cdot\mathbf{r}+\phi_\Delta)]\cos[1/2(\mathbf{k}_\Sigma\cdot\mathbf{r}-2\omega t+\phi_\Sigma)] , \quad (4)$$

where  $\Delta$  denotes difference and  $\Sigma$  denotes addition of the parameter (i.e.  $\mathbf{k}_\Delta=\mathbf{k}_1-\mathbf{k}_2$  and  $\mathbf{k}_\Sigma=\mathbf{k}_1+\mathbf{k}_2$ ). The fringe irradiance is imaged onto the observation screen as the observable quantity and is given by

$$I(\mathbf{r})=C_I|U(\mathbf{r},t)|^2=C_I|A|^2[1+\cos(\mathbf{k}_\Delta\cdot\mathbf{r}-\phi_\Delta)], \quad (5)$$

where  $C_I = \frac{1}{2}nc\epsilon_0$ ,  $n$  is the medium refractive index,  $c$  is the speed of light in a vacuum, and  $\epsilon_0$  is the permittivity of free space.

Note that the fringe modulation is in direction  $\mathbf{k}_\Delta$ . The fringe spacing  $\Lambda$  is

$$\Lambda=2\pi/||\mathbf{k}_\Delta||. \quad (6)$$

In Eqs. (1) through (6), effects of polarization are ignored. In this work, the angular subtense between  $\mathbf{k}_1$  and  $\mathbf{k}_2$  is very small, and the beams are of like polarization.

Therefore, any reduction in the fringe visibility resulting from polarization effects is insignificant and is ignored.

One of the simplest ways to demonstrate an interference pattern is implementing a classic Young's double-pinhole experiment. This type of interferometer samples the wavefront of a source at each of the two pinholes in the aperture (pinhole) plane, as shown in Figure 1. The model described here is an opaque screen with two tiny holes separated by a distance  $d_{ph}$  along the y-dimension. In this model,  $d_{ph}$  is small compared to the observation distance. The pinholes are typically on the order of microns in diameter. When illuminated with a plane wave, the pinholes produce approximately spherical wavefronts in transmission that interfere at the observation plane. For this model, the spherical waves at the observation plane are well approximated by  $\mathbf{k}_1$  and  $\mathbf{k}_2$  plane waves, and  $\mathbf{k}_\Delta \cdot \mathbf{r} \approx (2\pi/\lambda) \cdot \text{OPD}$ . The  $\text{OPD} = r_1 - r_2$  is the optical path difference between the paths from pinhole one ( $r_1$ ) and pinhole two ( $r_2$ ) reaching the observation point, as shown in Figure 4. In the observation region, straight-lined equally spaced cosine fringes are observed that are labeled with corresponding orders defined by  $m\lambda$ . The integer  $m$  corresponds to the number of wavelengths of OPD between the pinholes and the observation point. Detail of the YDPI is shown in Figure 4 with respect to the OPD

calculation. Note that  $OPD = \lambda(m+1/2)$  for the center of a dark fringe and  $OPD=m\lambda$  for the center of a bright fringe, and

$$\Lambda = \frac{\lambda z_0}{d_{ph}}. \quad (7)$$

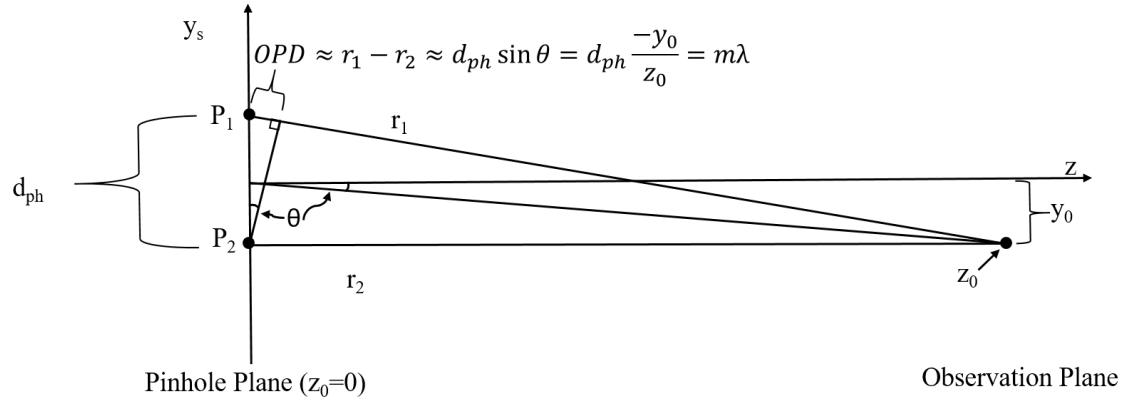


*Figure 4: The basic Young's double pinhole interferometer (YDPI) represented by two pinholes ( $P_1$  and  $P_2$ ) that are separated a distance  $d_{ph}$ . Wavefronts transmitted by the pinholes travel along the  $z$ -direction to the observation plane. The interference pattern is observed at the observation plane. Each fringe is labeled with corresponding orders of  $m\lambda$ , where  $m$  is an integer.[1]*

For typical experiments, a camera is used to observe the fringe pattern, where irradiance of the fringe pattern produces pixel values. For plane waves with amplitude  $A$ , irradiance is the square modulus of the electromagnetic field, which is

$$I(OPD) = C_I |U(OPD)|^2 = 2C_I |A|^2 [1 + \cos(\frac{2\pi}{\lambda} OPD)], \quad (8)$$

where  $C_I = (\frac{1}{2})cn\epsilon_0$ .

One of the most important characteristics of the fringe pattern is the fringe visibility, which is sometimes called fringe contrast. The fringe visibility is a very

important parameter of coherence theory that involves both spatial and temporal coherence. Spatial coherence is related to visibility reduction as a function of source size, whereas temporal coherence is related to fringe visibility as a function of source wavelength distribution. Visibility is defined in Figure 5 and Eq. (9), where minimum and maximum irradiance values of the fringe pattern are  $I_{\min}$  and  $I_{\max}$ , respectively. When the two interfering waves have unequal amplitudes or the source is not perfectly coherent,  $I_{\min} \neq 0$  and  $V < 1$ .

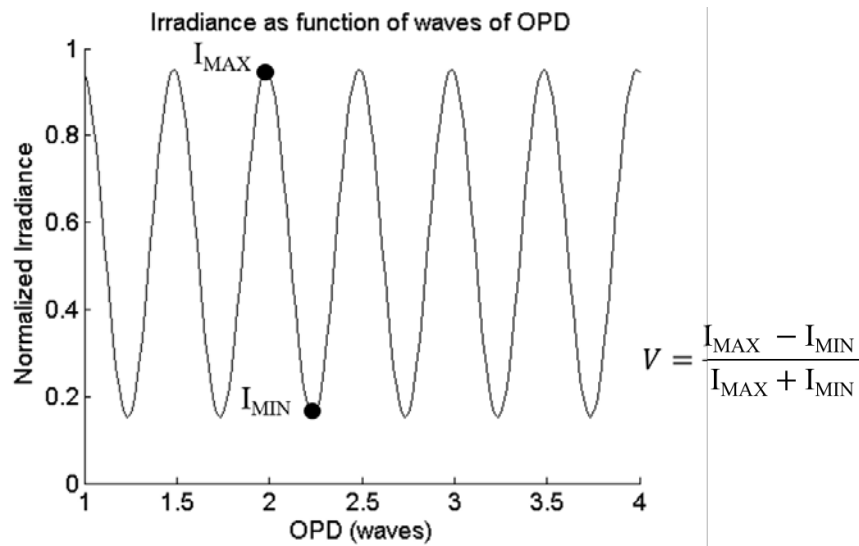


Figure 5: Irradiance profile associated with the visibility of the fringes in observation space. As shown,  $V=0.8$ .

In this work, the source is assumed to be nearly quasi-monochromatic, extended and incoherent, so only spatial coherence effects are considered. The equation relating fringe visibility to spatial coherence is

$$V\left(\frac{\theta_{ph}}{\lambda}\right) = \frac{(I_{max}-I_{min})}{(I_{max}+I_{min})} = 2 \frac{\sqrt{I_1 I_2}}{I_1+I_2} \mu_{12}^x\left(\frac{\theta_{ph}}{\lambda}\right). \quad (9)$$

The term  $\mu_{12}^x\left(\frac{\theta_{ph}}{\lambda}\right)$  is the spatial coherence visibility factor and is the dominant term in the expression for the visibility of fringes when the source bandwidth is narrow.[1] The “x” in the spatial coherence visibility term denotes the spatial dependence of the source. That is, observed visibility is due to the size of the quasimonochromatic incoherent extended source. The “12” represents interference resulting from two sample points (pinholes),  $\lambda$  is the mean wavelength of a quasimonochromatic source, and  $\theta_{ph}$  is the angular subtense of the pinholes as seen from the source, as shown in Figure 1. A vector describing the direction of the pinhole orientation in the aperture plane is

$$\mathbf{d} = d_{ph} \cdot \hat{\mathbf{d}}, \quad (10)$$

where  $\hat{\mathbf{d}}$  is simply the unit vector in the direction defined by a line connecting the two pinholes (see Figure 6). It makes no practical difference in which orientation  $\hat{\mathbf{d}}$  is assigned. Either  $1 \rightarrow 2$  or  $2 \rightarrow 1$  gives the same result. In this work, the extended quasimonochromatic source is an incoherent continuous source distribution. The source emission power distribution is measured in units of  $\text{Wm}^{-2}$  (power per unit area) and is known as the radiant exitance  $M(x_{src}, y_{src})$ . The total irradiance pattern in the observation plane is calculated by integrating the differential fringe patterns created by  $M(x_{src}, y_{src})$  from each  $dx_{src}dy_{src}$ . The normalized source radiant exitance distribution is

$$m_R(x_{src}, y_{src}) = M(x_{src}, y_{src}) / \iint M(x_{src}, y_{src}) dx_{src} dy_{src}. \quad (11)$$

Due to the Van Cittert-Zernike theorem and the nature of an extended quasimonochromatic source, the spatial coherence visibility factor at the observation plane is proportional to the absolute magnitude of the Fourier transform of the normalized source radiant exitance  $m_R$ , given by

$$\mu_{12}^x\left(\frac{\theta_{ph}}{\lambda}; \hat{\mathbf{d}}\right) = |\mathbf{F}_{\hat{\mathbf{d}}}\{m_R(x_{src}, y_{src})\}| = \iint m_R(x, y) \exp(-j2\pi(\xi x + \eta y)) dx_{src} dy_{src}, \quad (12)$$

where  $\vec{\xi} = \frac{\theta_{ph}}{\lambda} [\alpha_d \hat{x} + \beta_d \hat{y}]$ ,  $\hat{x}_{src} = x_{src} \hat{x} + y_{src} \hat{y}$ ,  $\hat{\mathbf{d}} = \alpha_d \hat{x} + \beta_d \hat{y}$ , and  $(\alpha_d, \beta_d)$  are direction cosines describing the direction of  $\mathbf{d}$  in the aperture plane. [1] That is, the value of  $\mu_{12}^x$  is determined from the origin of the two-dimensional Fourier transform in the direction  $\hat{\mathbf{d}}$  at a distance  $\frac{\theta_{ph}}{\lambda}$ .

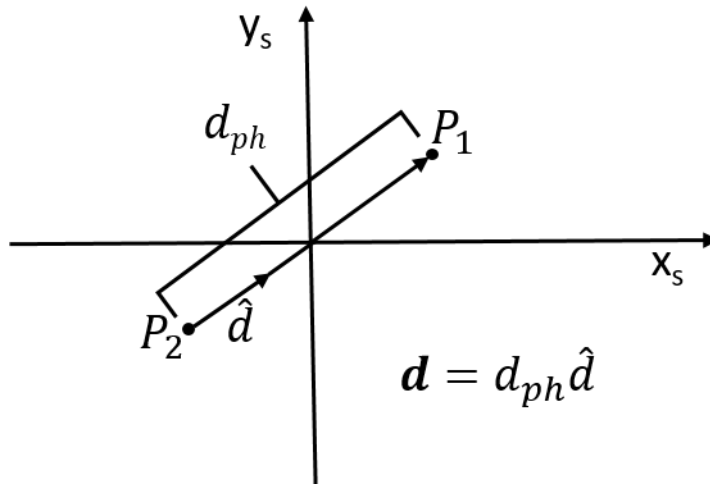


Figure 6: Illustration of the projection vector  $\mathbf{d}$  between the displacements of two pinholes (black dots).



Different techniques have been used to measure spatial coherence of sources, including the use of uniformly redundant arrays.[10] One particular study uses the Young's Double Pinhole Interferometer (YDPI) and an aperture with differently spaced pinhole pairs to measure the complex degree of spatial coherence for an incoherent quasi-monochromatic source at a wavelength of 632.8nm. Six pinhole pairs are generated from a mask fabricated with four pinholes. The complex degree of spatial coherence are measured for pinhole distances of 1.5, 4.5, 9.0, 10.5, 13.5 and 15.0 millimeters.[11] Temporal coherence properties of light-emitting diodes (LEDs), including coherence length (the OPD distance between the fringe with maximum visibility to first region with minimal visibility) and the spectral coherence (spatial coherence at a particular frequency) were investigated for a red and green LED with wavelengths of 641nm and 545nm. To determine the spectral coherence, Dalip Sing Mehta et al used a YDSI to record several different interferograms. The visibility of the fringes are measured by recording several interferograms for four different slit separations: 400, 800, 1100, and 1650 $\mu\text{m}$ . The spectral coherence for the red LED is 0.85 at a 400 $\mu\text{m}$  slit separation and 0.8 for the green LED at 500 $\mu\text{m}$  slit separation.[12] Popmintchev *et al.* uses HHG supercontinuum X-rays from the excitation of He-Ne gas from a 3.9 micron laser and a YDSI to study coherence of a supercontinuum laser. Fringe visibility is measured with slit widths of 5 $\mu\text{m}$  and slit separation of 10 $\mu\text{m}$ . [13] An aperture called a uniformly redundant array (URA) has been used to measure spatial coherence of an undulator radiation (high energy x-rays) source at the Advanced Photon Source at Argonne

National Laboratory and is measured for discrete slit widths of 10, 50, 90 and 170 microns. The URA is a complex mask that contains all the aforementioned slit widths with slit separations ranging from 0 to 700 $\mu\text{m}$  so that every slit separation acting as an independent YDSI for each slit width is measured only once. The mask is phase shifting since it exhibits a  $\pi$  phase shift for the metallic component of the aperture. [14] A HHG beam generated from a 790nm femtosecond laser was measured with 20-50 $\mu\text{m}$  pinholes in a YDPI with pinhole spacings of 142, 242, 384 and 779 microns to measure the spatial coherence. [15]

The present study conducts models and experiments to determine the coherence effects from a near ultraviolet (NUV) LED as the diameter of the source is changed. Piecewise diffraction theory is used to model the system in order to determine the optimal distance for high sensitivity with the use of an x-shaped aperture.

## CHAPTER 4: THEORY

The x-shaped aperture is effectively a collection of pinholes with varying spacing, as shown in Figure 7. Each position along the x direction effectively forms a YDPI, even though the aperture is fabricated as a double slit oriented in an x shape.

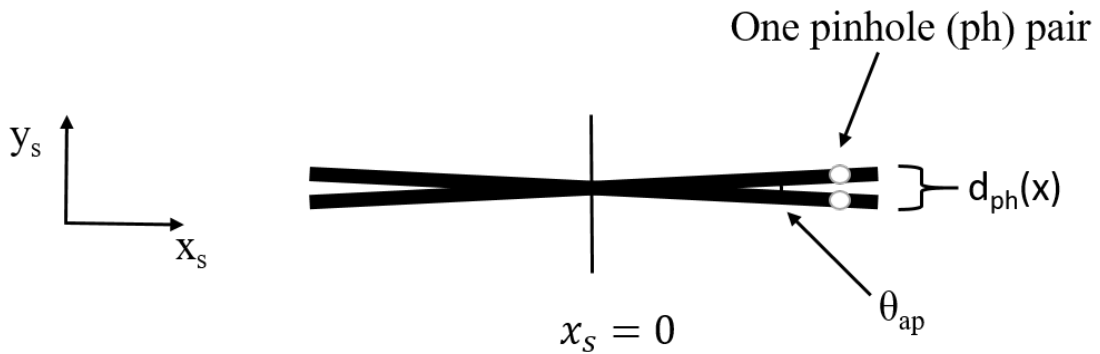


*Figure 7: Concept of the x aperture as a collection of pinholes with different spacings. Black represents the open portion of the aperture.*

Conceptually, the “x” is a collection of finely sampled pinholes with different spacings. Starting at  $x_s=0$  and moving in the positive  $x_s$ -direction, the spacing between each pinhole pair becomes larger. Each pinhole pair acts as a single YDPI with its corresponding spacing  $d_{ph}$ , which produces a fringe pattern in the observation plane. Since each pinhole pair produces fringes with spacing  $\Lambda$  as defined by Eq. (7). At distance  $z_0$  from the aperture, the net effect is a fringe pattern with

$$\Lambda(x_0) = \frac{\lambda z_0}{\theta_{ap} x_0}, \quad (13)$$

as shown in Figure 8. The fringe lines form a family of equally-spaced hyperbolas in each quadrant with the coordinate axes as their asymptotes.

The LED source is assumed to have a narrow spectral distribution that would not introduce any additional fringe visibility reduction from the expected OPD for each pinhole pair in the experiment. The bandwidth ( $\Delta\lambda=25\text{nm}$ ) of the commercially available LED (ENGIN #LZ4-00U600) can be further limited ( $\Delta\lambda=10\text{nm}$ ) using an optical filter (TECHSPEC Hard Coated OD 4 #65-069), if necessary. The LED operates at a mean wavelength of 365nm. The  $\Delta\lambda=25\text{nm}$  bandwidth corresponds to a coherence length  $l_c = 5.3\mu\text{m}$ . The ratio of the coherence length to wavelength suggests a maximum of 29 visible fringes in the observation plane. The first  $\pm 7$  orders are shown in Figure 8, which are the central 15 fringes. In practice, only the central 4 or 5 orders are used in the measurement, so temporal coherence effects are not considered. The fringe pattern is observed close to the aperture in the Fresnel region.

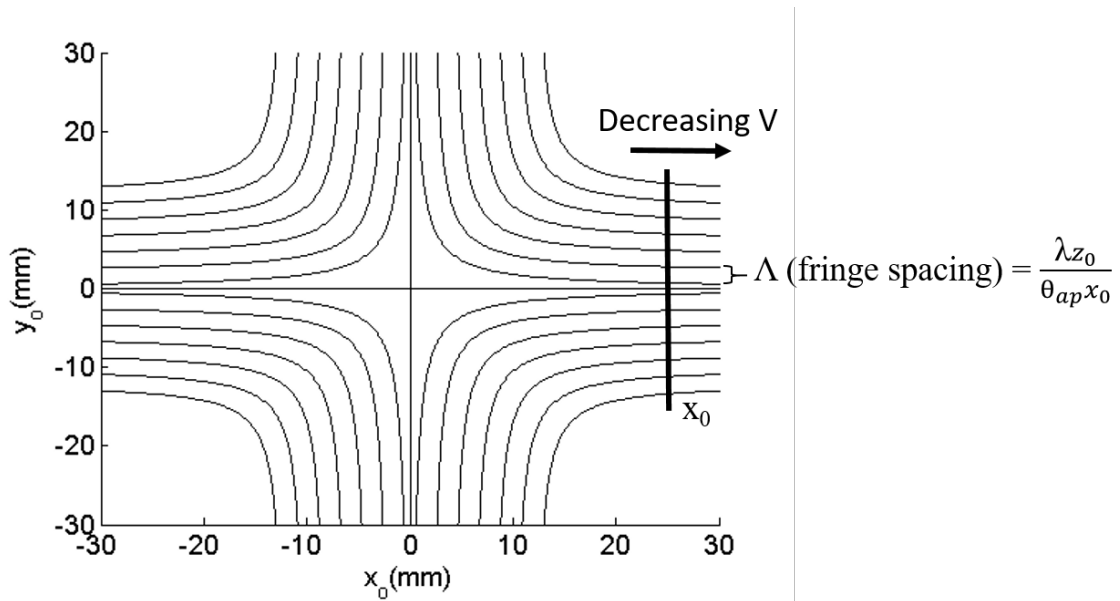


Figure 8: Irradiance pattern at the observation plane is a family of hyperbolas with the coordinate axes as their asymptotes.  $\Lambda$  is proportional to  $\frac{1}{x_0}$ .

A finite-size source produces reduced visibility as  $d_{ph}$  increases, so the fringe visibility in Figure 8 decreases with increasing fringe spatial frequency along the positive  $x_s$ -direction from  $x_0=0$ . This work shows how these concepts are used to accurately determine spatial properties of the source. The overall net effect is a decrease in visibility as the distance from the center of the  $x$  aperture increases. The rate of visibility decrease is proportional to the size of the source.

The normalized source radiant exitance  $m_R(x_{src}, y_{src})$  is modeled using small, square piecewise continuous sections. It is assumed that each section in the source propagates

light coherently to the x aperture. In the aperture plane, the field is divided into small square sections, as shown in Figure 9.

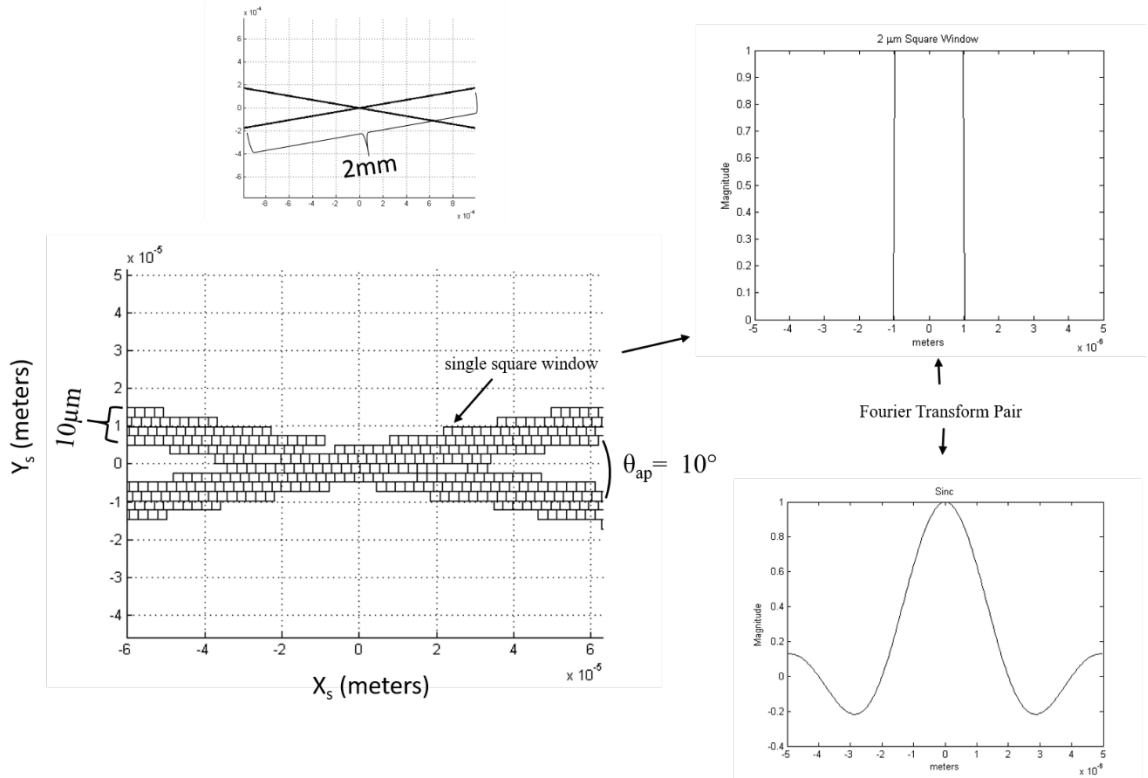
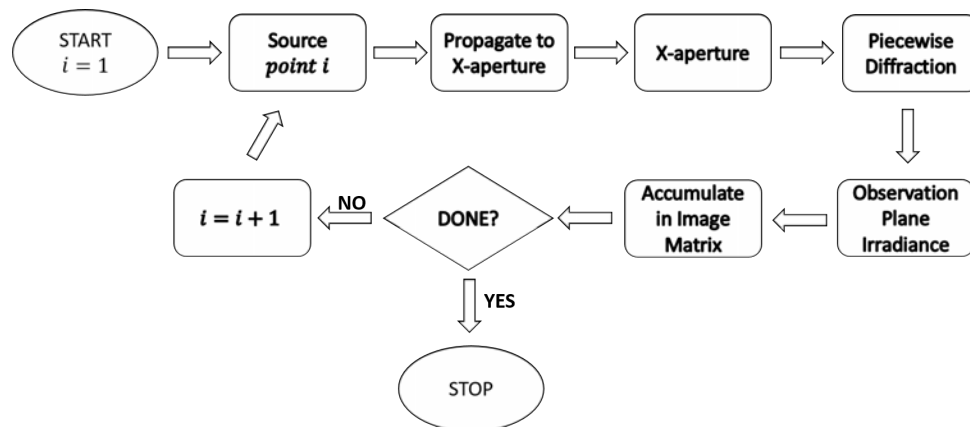


Figure 9: Model of piecewise rectangular surfaces forming the geometry of the x aperture in the region of the center near  $x_{0=0}$  (left). Illustration of a rectangular function and its Fourier transform, the sinc function, as a Fourier Transform pair (right). The slit is 2mm in length (but only the central  $\pm 6\mu\text{m}$  are shown) 10 microns in width, and  $\theta_{ap}$  is 10 degrees.

Piecewise diffraction is used from the aperture to the observation plane. Fields from each of the square aperture windows propagate to the observation plane through Fraunhofer diffraction, because the square windows in the x aperture are small enough (on the order of microns) so that the conditional  $N_f$  (Fresnel number)  $< 0.1$  is satisfied at

the observation plane distance  $z_0$ . Linearity of the fields allows simple addition of the fields from each window. The Fourier transform relationship of the Fraunhofer approximation implies a two-dimensional “sinc” function field distribution at the observation plane that is geometrically centered at the corresponding window. After fields from all x-aperture windows are added, the square magnitude of the result yields the irradiance expected from the source section. The same calculation procedure is used for the remaining source sections in  $m_R$  with the irradiance patterns added to yield the total irradiance. Since the source is incoherent, there are no cross terms in combining irradiance patterns. A flow chart of the simulation is in Figure 9.



*Figure 10: Flow chart illustrating the sequence of simulating the propagation of the electric field from source plane to observation plane.*

To simulate the optical system, a model is created in the program Optiscan, which operates in the Matlab environment. The simulation considers several key design parameters for the x aperture (see Table 1):

<b>Design Parameters</b>	<b>Description</b>
$\theta_{\text{ap}}$ (degrees)	Angle between the slits
$\mathbf{a}$ ( $\mu\text{m}$ )	Slit width
$\mathbf{l}$ ( $\mu\text{m}$ )	Slit length

*Table 1: Design parameters for the x aperture.*

The optical setup includes the x aperture designed with specific parameters and small circular disk source sizes ( $D_{\text{src}}$ ) ranging from 0.5mm to 2.5mm, in 0.5mm increments. This incoherent quasimonochromatic source is placed at a distance of 1m from the x-aperture ( $z_{\text{src}}$ ). The source has a wavelength  $\lambda$  of 365 nm, and  $\Delta\lambda=13\text{nm}$  with an x-aperture pixel pitch of 2.1 $\mu\text{m}$ . The pixel pitch value derives from the resolution limit of the Maskless Lithography Tool (MLT) used to fabricate the aperture. [16]

### **Discussion of Parameters**

#### *Observation Plane Distance*

The distance from aperture to observation plane ( $z_0$ ) is limited by two factors. First, the camera (Kingfisher ICX694) for data collection restricts the propagation length from aperture to observation plane to a minimum distance of 2 cm. This minimum is due to mechanical limitations from a recession to the pixel array plane of the camera. Also, the visibility fit to the visibility data from the simulation becomes worse as  $z_0$  increases, as shown in Table 2. Initially,  $\theta_{\text{ap}}$  is fixed at a value of 15°, which corresponds to a range



of pinhole separation values  $d_{ph}$  between 0.10 mm and 0.33 mm. The slit width  $a$  is fixed at  $10\mu\text{m}$ . The length  $l$  is fixed at 1mm. Results from the fit in Table 2 suggest that 2 cm is the optimal  $z_0$  based on the error of the diameter of the source from its true value,

$$D_{error} = D_{src} - D_{calc} \quad (14)$$

Source Diameter Error						
$Z_0$ (cm)	$D_{src}$ (mm)					
	0.5	1.0	1.5	2.0	2.5	
2	0.10	0.14	0.14	0.165	0.144	$D_{error}$ (mm)
3	0.16	0.16	0.216	0.145	0.168	
4	0.16	0.16	0.153	0.145	0.368	
5	0.16	0.17	0.16	0.145	0.164	
6	0.16	0.18	0.166	0.47	0.468	
7	0.18	0.19	0.173	0.51	0.452	

*Table 2: Results from fitting the visibility data in the simulation to the theoretical value showing the error in source diameter as a function of observation plane distance and source size.*

#### *Slit Width*

In a YDPI or YDSI, the light undergoes two effects: diffraction and interference. The irradiance pattern is the combination of these two phenomena, where the slit width determines the angular distribution of the diffracted light and modulates the interference pattern at the observation screen. The interference term, as shown in Eq. (15), is enveloped with the diffraction term of Eq. (16). The product of the interference term and

the diffraction term yields the total irradiance pattern as a function of distance along the observation plane. In some cases an interference maximum coincides with a diffracted minimum, in which case no fringe for that particular order is observed. Also, the closer the slit width  $a$  is to the wavelength, the wider the central lobe becomes, and less light into the central diffraction lobe is allowed through the slit. Guided by the aforementioned statements and Eqs. (15)-(18), the slit width  $a$  is set to a value that optimizes  $w$  the zero-to-zero width for the central lobe of the diffraction pattern, fit to the dimensions of the camera array. Consideration for the minimum feature width that can be printed by the MLT is also a factor in determining slit width.

$$I = I_0 \cos^2 \left( \frac{\pi d_{ph} \sin \theta}{\lambda} \right) \quad (15)$$

$$I = I_0 \operatorname{sinc}^2 \left[ \pi a \sin \left( \frac{\theta}{\lambda} \right) \right] \quad (16)$$

$$I_{total} = I_0 \cos^2 \left( \frac{\pi d_{ph} \sin \theta}{\lambda} \right) \operatorname{sinc}^2 \left[ \pi a \sin \left( \frac{\theta}{\lambda} \right) \right] \quad (17)$$

$$w = \frac{2\lambda z_0}{a} \quad (18)$$

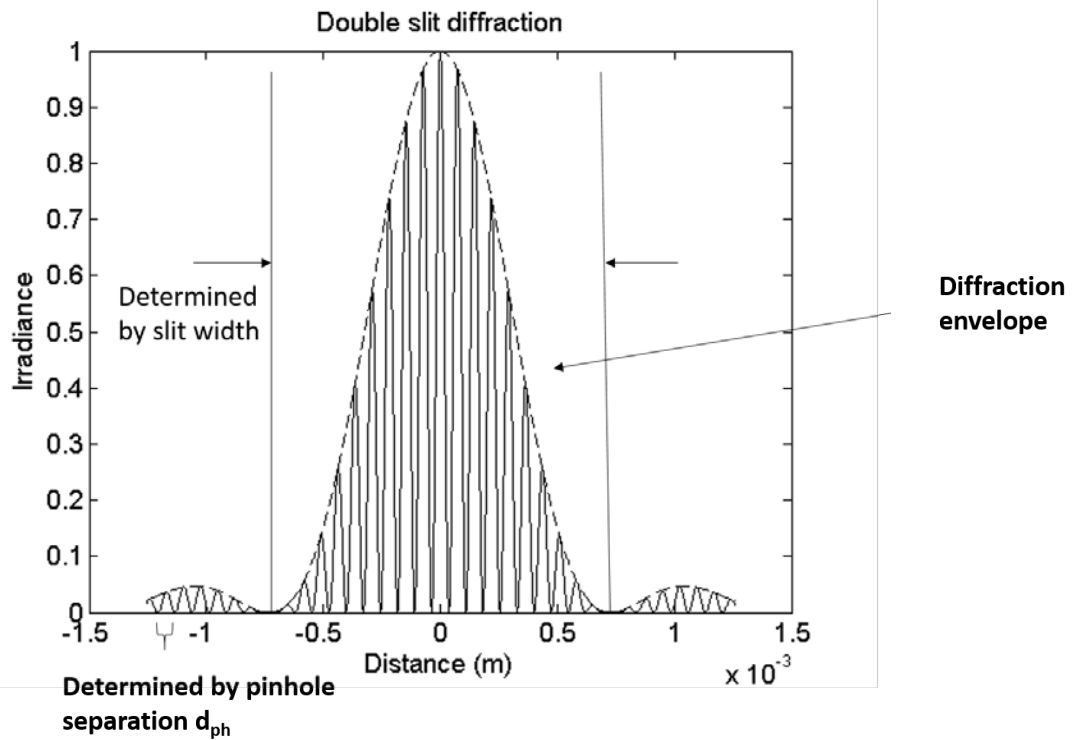


Figure 11: The intensity pattern for a double slit interferometer. The diffraction term envelopes the interference term governed by the slit width and pinhole separation, respectively.

A  $10\mu\text{m}$  slit width is nearly the finest features that can be fabricated by the MLT. The zero-to-zero width of the central lobe is  $1.46\text{mm}$  for  $a=10\mu\text{m}$ , while the camera supports a  $12.5\text{ (H)}$  by  $10\text{mm (W)}$  active area. Five diffraction orders are observed in the image plane. Now that the slit width is fixed, the angular separation of the slits are determined.

*Angular separation of slits*

The value of  $\theta_{ap}$  is chosen such that each effective pinhole separation is small enough to induce interference effects at the observation plane with reasonable fringe spacings  $\Lambda$ . The initial value at determining  $\theta_{ap}$  is  $15^\circ$ , and the value is decreased to a new value of  $\theta_{ap} = 10^\circ$  to achieve a range of pinhole separation between 0.1 mm and 0.3 mm. This value yields a useful diffraction pattern with enough fringes inside the dimensions of the camera to accurately calculate the visibility. This result is determined by obtaining a fringe spacing, governed by Eq. (13), to be on the order of tens of microns. The fringe spacing on the observation plane in the simulation has a range of  $[24\mu\text{m}, 52\mu\text{m}]$ , which is reasonable considering the camera pixel spacing is  $4.54\mu\text{m}$ .

In summary, the parameters corresponding to observation distance, slit width and angular slit separation are engineered one at a time to optimize ideal experimental conditions. The observation distance  $z_0$  is limited to 2cm. The x aperture design parameters are as follows: slit width  $a = 10\mu\text{m}$ , slit length  $l = 2\text{mm}$ ,  $d_{ph} = 0.1\text{mm}$  to  $0.3\text{mm}$  and  $\theta_{ap} = 10^\circ$ .

The optical design includes five key components. First is the ENGIN 365nm UV LED (LZ4-00U600) source, which is placed directly behind a spatial filter. Placed approximately 1m away from the spatial filter is the x aperture. The interferogram is collected on a Kingfisher camera (ICX-694) which is connected to the computer. Appendices B and C list the source and camera specifications, respectively. A schematic showing the optical design is shown in Figure 12.

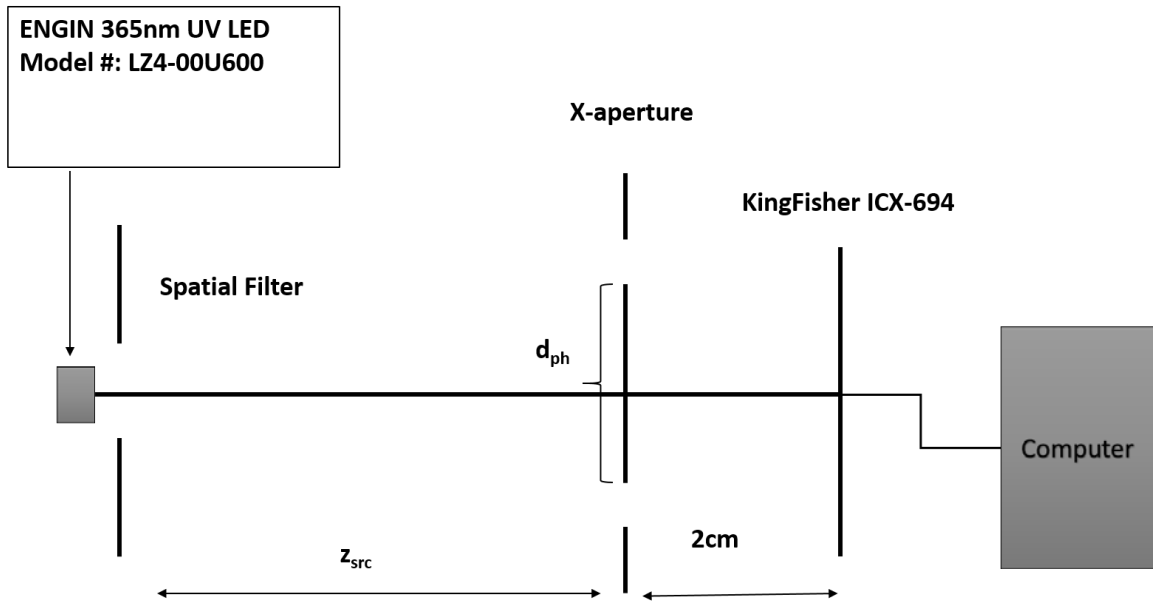


Figure 12: The optical design for coherence analysis of an x-aperture. Dimensions of the x aperture are greatly exaggerated in this figure.

The simulation propagates a light field through the optical design and yields a family of hyperbolic fringes seen in Figure 13.

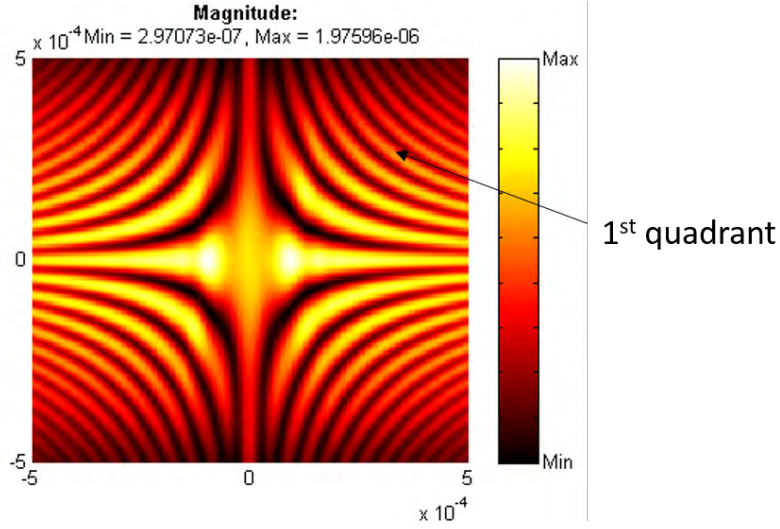


Figure 13: Family of hyperbolaes after simulation through optical system at a wavelength of 365 nm.

The irradiance pattern is symmetrical about the axes, so simulation of one quadrant is sufficient to understand characteristics of the device. If the source is circular, then the appropriate model for geometry of the source is a circ function, which is defined as

$$m_R(r_{src}) = \frac{4}{\pi D^2} \text{circ} \left( \frac{r_{src}}{D} \right) \quad (19).$$

The Fourier transform of Eq. (19) is the sombrero function,

$$\mu_{12}^x \left( \frac{\theta_{ph}}{\lambda} \right) = \mathbf{F}_{\frac{\theta_{ph}}{\lambda}} \left[ \frac{4}{\pi D^2} \text{circ} \left( \frac{r_{src}}{D} \right) \right] = \text{somb} \left( D \frac{\theta_{ph}}{\lambda} \right) \quad (20).$$

Each column in the matrix of the hyperbolic irradiance pattern is scanned for minimum and maximum values. These parameters are used for calculating the visibility.

Visibility reduces when the source size  $D_{src}$  increases with  $\frac{\theta_{ph}}{\lambda}$  constant, as seen in Eq.

(20) from the dependence of the term  $\frac{\theta_{ph}}{\lambda}$  in the spatial coherence visibility factor. A Matlab© program is developed that optimizes the fit to the calculated visibility pattern observed in the model of the optical system in order to determine source size. A flow chart of the routine is shown in Figure 14, and the program is listed in Appendix A.

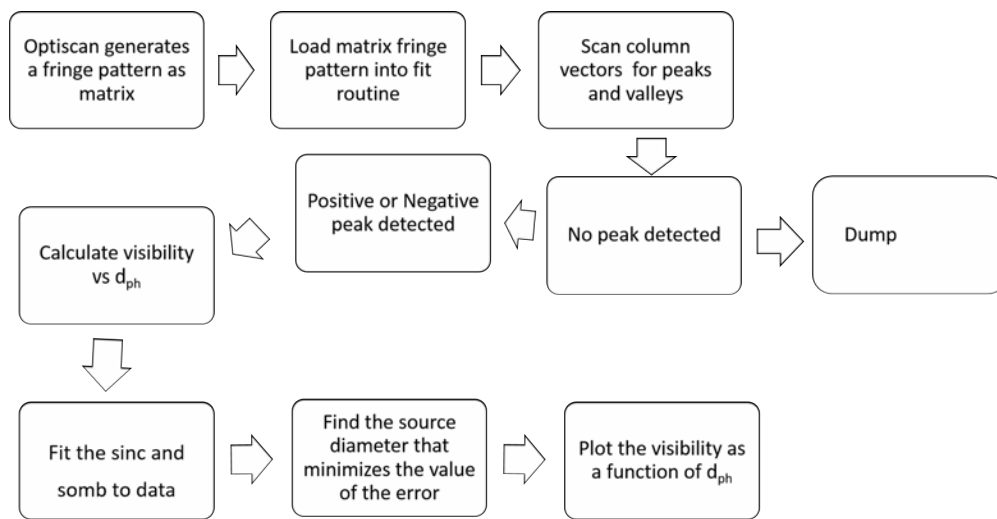


Figure 14: Flow chart showing the process of the fitting routine for finding a source diameter.

The flow chart in Figure 14 shows the process of the fitting routine in order to determine a source diameter. The fringe pattern generated from OptiScan is loaded into the fit routine as a matrix. It scans each column in the fringe pattern for intensity minima and maxima. If no minimum or maximum is found, then the data is discarded. If a corresponding peak and valley exists in the data, then it is used to calculate visibility. This calculation is repeated for each pinhole separation moving along the positive  $x_0$ -

direction from the origin (center of  $x$ ). The sombrero or sinc pattern generated from the calculation of visibility is then fit to the data collected from Optiscan. The source size is calculated from the width of the sombrero function. Figure 15 displays two subset figures describing the part of the process of how the visibility is calculated from the resulting interferogram from OptiScan. On the left of Figure 15 is a snapshot from the sinusoid corresponding to the fringe pattern in column 113 of the input matrix. Notice the peaks and valleys associated with the minimum and maximum irradiances are used to calculate the visibility. On the right of the same figure is the fringe pattern showing column 113 indicated by the vertical black line.

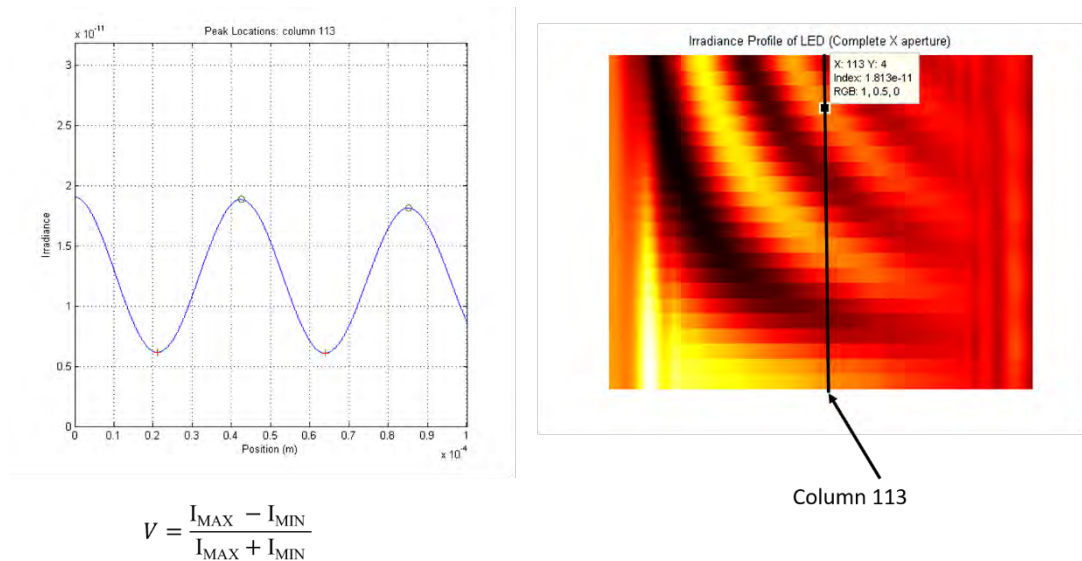


Figure 15: The irradiance profile (as a function of OPD) of column 113 shown on the left. The first quadrant of the interferogram on the right is produced from the  $x$ -aperture for a 1.5 mm source diameter with a  $\lambda=365$  nm ( $\Delta\lambda = 10$  nm) and  $\theta_{ap}=20^\circ$ .



Figure 16 shows the visibility curve as a function of pinhole distance for the best fit sombrero and sinc functions. The sinc and sombreros generated are fit to the data stored in OptiScan, showing a linear relationship between the pinhole separation and visibility. Therefore, visibility, which is used to determine coherence, decreases with increasing pinhole separation. Note that the  $x_0$  axis does not start from zero, due to the diffractive features around the origin.

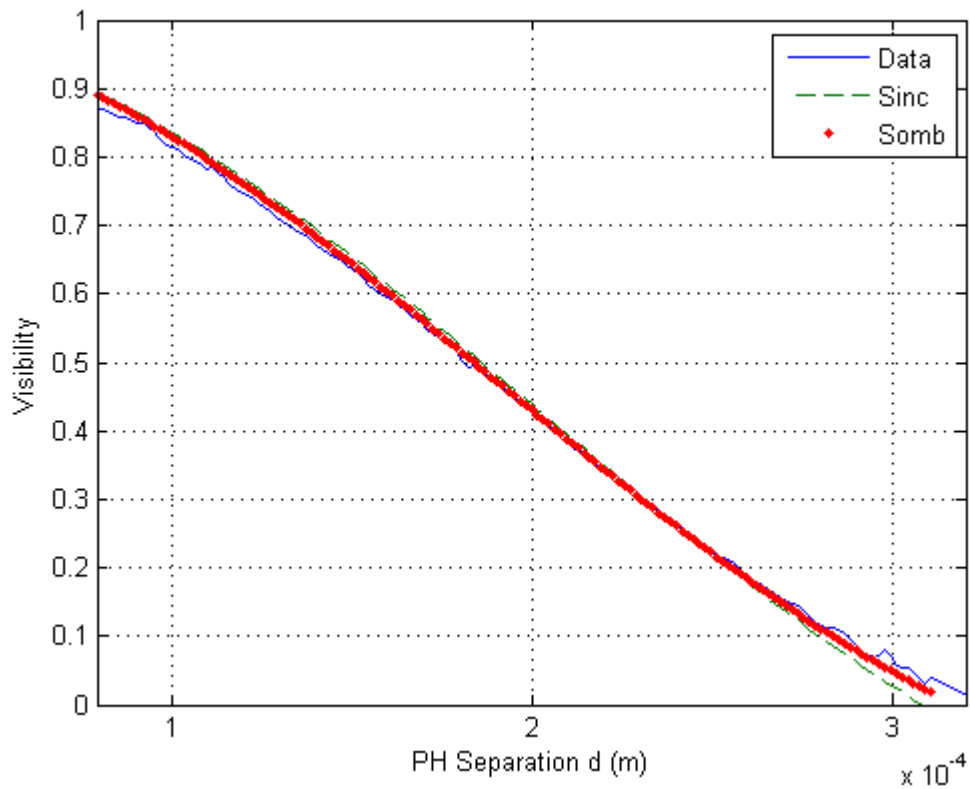
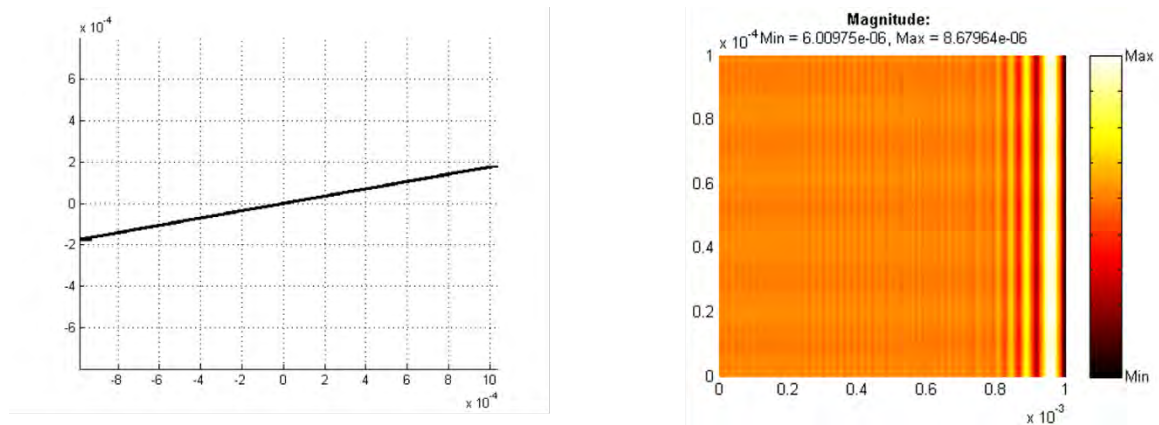


Figure 16: Results from the simulated LED showing visibility as a function of pinhole distance  $d_{ph}$ . The best fit sombrero and sinc functions are also shown.

In Figure 17, in the far right portion of the interferogram, there is a noticeable pattern of straight-lined equally spaced cosine modulated fringes with irradiance that increases linearly. This increase seems to be related to the tilt of slits in the aperture. Along the slit in the direction of increasing  $x$  there is an increase in intensity of the spurious fringes. This is visibly shown in Figure (15), which has one 10 micron width slit tilted at an angle of 10 degrees ( $\theta_{ap}=20^\circ$ ) relative to the  $x$ -axis at a wavelength of 362 nm. This spurious fringe may produce background in the experiment.



*Figure 17: (Left) One 2 mm long, 10 micron thick slit tilted at an angle of 10 degrees relative to the  $x$ -axis illuminated with a 362 nm wavelength. (Right) Simulation of Interferogram resulting from the aforementioned process.*

The figure of merit for fitting somb or sinc curves to the simulation is the root mean square (rms) variation between the visibility as a function of  $x_0$  from the simulation and the visibility calculated from the sinc/somb fit in Figure 14. To find the rms, a subroutine calculates the square root of the sum of the difference of squares between the fit routine's visibility and the Optiscan© simulation with the expression,

$$\sigma_{rms} = \sqrt{\sum_{i=1}^N \frac{(V_i - V_{fit})^2}{N}} \quad (21),$$

where  $V_i$  are from the simulation and  $V_{fit}$  is the functional value from the sinc or somb functions. For example, results from the simulation and fitting routine of a 1.5 mm diameter incoherent quasimonochromatic disk source with a wavelength of 365nm (calculated as a weighted sum between 359 nm and 371 nm) propagating one meter away to an x-shaped aperture with a 10 $\mu$ m and then 2 cm to the observation plane, yields a 1.40 mm diameter source, and the sinc fit for comparison yields a 1.17 mm diameter.

In summary, OptiScan simulates the propagation of the light field transmitted through an x shaped aperture modeled with ten micron pinholes by varying spacing to the observation screen yielding a family of hyperbolae that are symmetrical about the x and y axes. The first quadrant of the interferogram is scanned for minimum and maximum intensities to calculate visibility. The fit routine achieves a fit to 6.7% of the actual value in an example using a 1.50 mm source diameter. There also appears to be spurious straight-lined equally spaced cosine modulated fringes with increasing intensity along the x-axis that may contribute to noise. These fringes seem to come from the tilt related to one slit in the aperture. The next chapter discusses the detail in experimentation for the x-aperture interferometer.

## CHAPTER 5: EXPERIMENTAL RESULTS

Experimental verification of the x-aperture concept for determining effective source size is presented in this chapter. The first section of the chapter discusses the fabrication of the materials with explanation of their use. The next section covers the experimental setup with the results. The chapter concludes with a discussion of possible sources of error that contribute errors in source size fits to the spatial coherence being measured.

### *Fabrication*

The x-aperture is fabricated using the MLT using chromium on glass substrates in the geometry of an “X” (two slits on top of one another and angled with respect to the  $x_s$ -axis). The dimensions of the slit legs are 2mm long at an angle  $\theta_{ap}=20^\circ$ . The absence of the chrome on the substrate corresponds with the transparent component of the aperture. Four different x-apertures are produced for the experiments. Two x-apertures contain slit widths of  $10\mu\text{m}$  and two contain  $12\mu\text{m}$  slit widths. One of the  $10\mu\text{m}$  and one of the  $12\mu\text{m}$

slit width x-apertures has an entire “x” shaped geometry (transparent center section). The two remaining x-apertures have the center section of the “x” completely opaque or blocked out with no transmission of light. This blocked structure is illustrated in Figure 18.

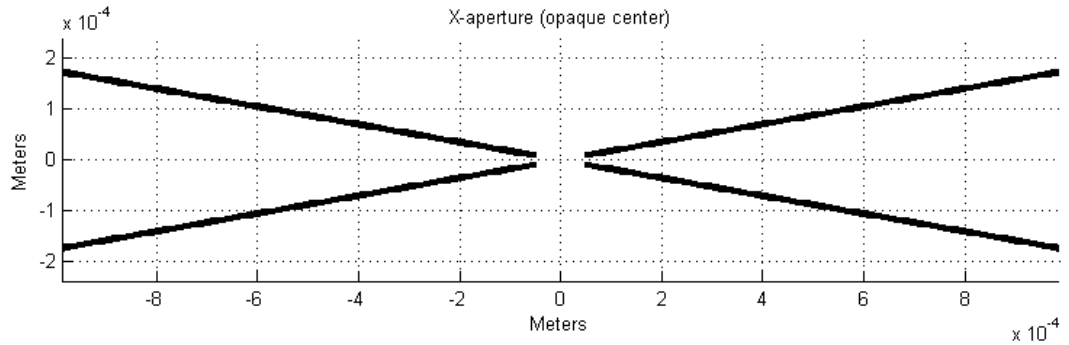


Figure 18: Illustration of X aperture without a center section (blocked).

Table 3 below summarizes the x-apertures that were fabricated for the experiment.

Label	X-Aperture Slit Widths	Center of X-Aperture
S <sub>1</sub>	10 μm	Blocked
S <sub>2</sub>	10 μm	No Block
S <sub>3</sub>	12 μm	Blocked
S <sub>4</sub>	12 μm	No Block

A finished product of an

Table 3: Four x-apertures fabricated. Two 10 micron apertures and two 12 micron apertures are presented, where one of each slit width size has a blocked center section to prevent any transmission of light.

x-aperture fabricated by the MLT is shown in Figure 19.

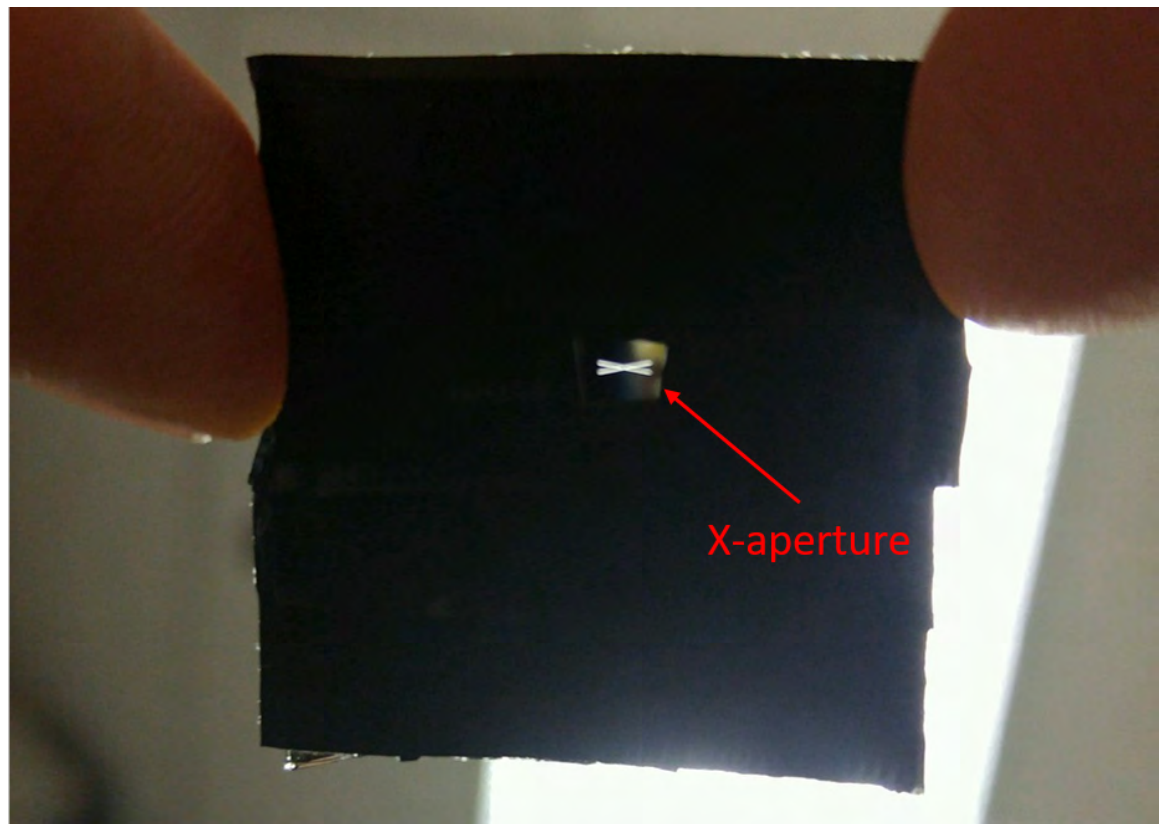


*Figure 19: A picture of an X-aperture that shows the relative size of the aperture. The remaining glass substrate not used in the experiment is covered with black electrical tape to prevent any unwanted transmission of light.*

In addition to the four x-apertures, three additional circular apertures are fabricated with sizes of 0.5 mm, 1.0mm, and 1.5mm in diameter. These source sizes are listed in the Table 4. The circular apertures act as spatial filters for the source. In other words, the size of the LED is limited with the circular apertures to agree with the simulation source sizes.

<b>Label</b>	<b>Circular Aperture Sizes</b>
$C_1$	0.5 mm
$C_2$	1.0 mm
$C_3$	1.5 mm

*Table 4: Three different circular apertures that range from 0.5mm to 1.5mm.*

An interferogram is produced for each circular aperture listed with each of the four x-apertures. Therefore, twelve experimental iterations are implemented to account for all combinations of x-apertures and source diameters.

### *Results*

The experimental setup includes an optical track, a stage, three circular apertures, four x-apertures, a rectangular optical mount (2), Mounting posts (3), 365 nm UV LED (#LZ4-00U600), and a CCD Camera (Kingfisher ICX694) connected to a computer. The

LED, mounted on a block, is placed one meter away from the x-aperture. The x-aperture is fixed on the rectangular optical mount and that rectangular mount is fixed on a mounting post. The x-aperture is placed directly in front of the camera. A picture of the entire setup is shown in Figure 18.

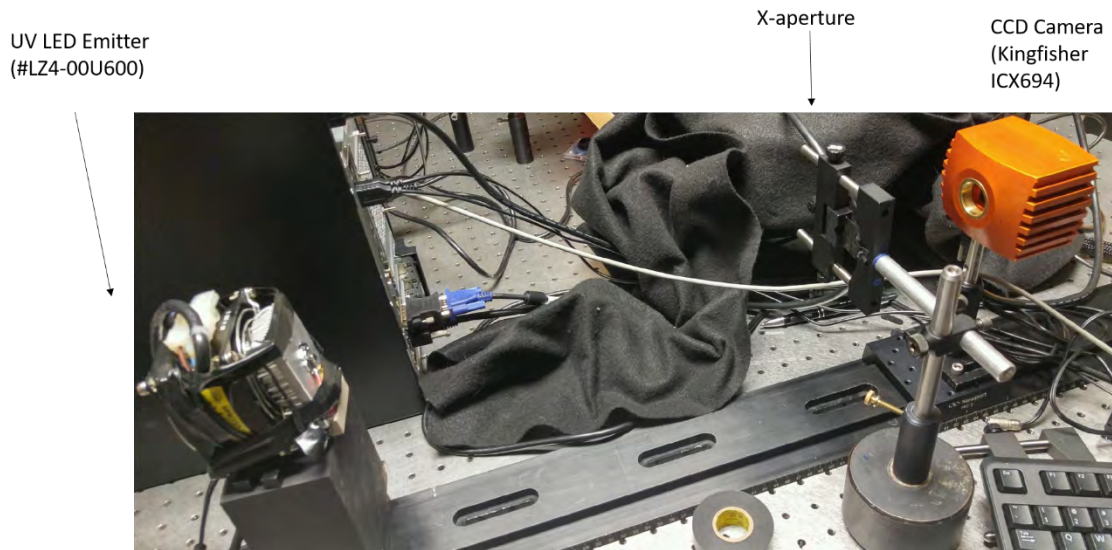


*Figure 20: The x-aperture setup includes an optical track, UV LED, CCD camera, mounting post, rectangular mount, and stage.*

Each iteration produces a gray-scale image on the camera array, as shown in Figure 22. The images of the fringe pattern at the CCD camera are very similar to the simulations with OptiScan in Matlab, as shown in Figure 13. After measurement each interferogram is loaded into the fit routine.

Due to the wavelength distribution of the source, temporal effects relating to the wavelength distribution of the source wash out the fringe visibility calculated in the fit



routine when an entire quadrant is scanned and high fringe orders  $m$  are used in the fit routine. Temporal coherence is the correlation between the decrease in visibility due to the power (frequency) spectrum of the source. At a mean wavelength ( $\bar{\lambda} = 370nm$  and bandwidth  $\Delta\lambda = 25nm$  the coherence length,

$$l_c = \frac{\bar{\lambda}^2}{\Delta\lambda}, \quad (22)$$

is found to be approximately  $5.3\mu m$ , where the coherence length is defined by the distance between the fringe with maximum visibility to the fringe with minimum visibility. The number of fringes one can observe in this situation before the fringe visibility is at a minimum can be found by evaluating the ratio of the coherence length  $l_c$  and the center wavelength  $\bar{\lambda}$ . This value evaluates to approximately fourteen fringes. As mentioned in Chapter 4, the initial assumption was that temporal effects, which affect  $y_0$ , would not be significant. However, experimental results indicate that using  $m > 3$  significantly affect fit accuracy. Therefore, a slight modification to the fit routine script is implemented, where smaller  $y_0$  image area centered around the  $m = 0$  order fringe is selected. In other words, only three to five fringes above and below the x-axis, are included in the visibility calculation inside of the fit routine, as shown in Figure 2. To give the reader a better understanding of what is meant by the author, see Figure 22.

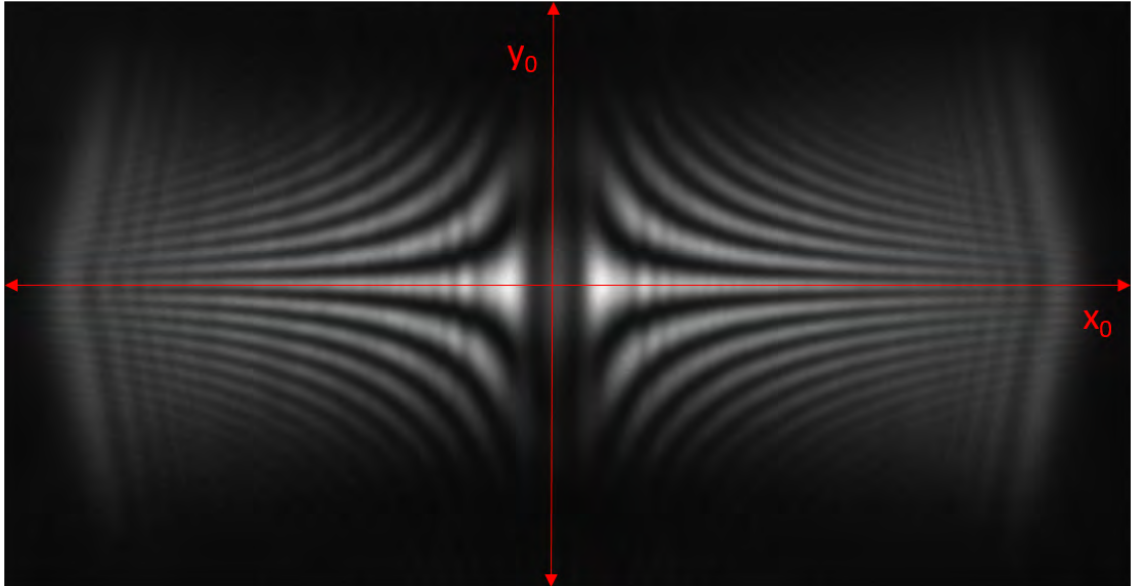


*Figure 21: Gray-scale image of the interferogram resulting from a 1.5mm circular aperture and a 12 micron x-aperture with a blocked center section. The images are enlarged to clearly observe the fringe contrast. Two image areas were selected to be scanned for visibility calculation. Starting from the  $x_0$ -axis (corresponding to the  $m=0$  fringe) a selection of three to five fringes in the  $y_0$  range above and below the  $x_0$ -axis are scanned for calculation of visibility in the fit routine.*

The stray light in the background of the images (not visible) is canceled out in order to not have an effect on the visibility. This cancellation is simply done by selecting an image area furthest away from the fringe pattern and subtracting the value of its irradiance from the irradiance in the image area that is scanned.

In Figures 22 and 23, there is a side-by-side comparison of the left and right image areas on each side of the  $y_0$  axis and their respective fits. Figure 22 shows the worst fits from a 0.5mm circular aperture ( $C_1$ ), 12 $\mu$ m slit widths and an x-aperture with a blocked center section ( $S_3$ ). The image areas are trimmed to the  $y_0$  range in order to avoid

temporal coherence effects. Figure 23 shows the best two fits corresponding to a 1.5mm circular aperture ( $C_3$ ) and a 12 $\mu\text{m}$  x-aperture containing a blocked center section ( $S_3$ ) of the “x”.

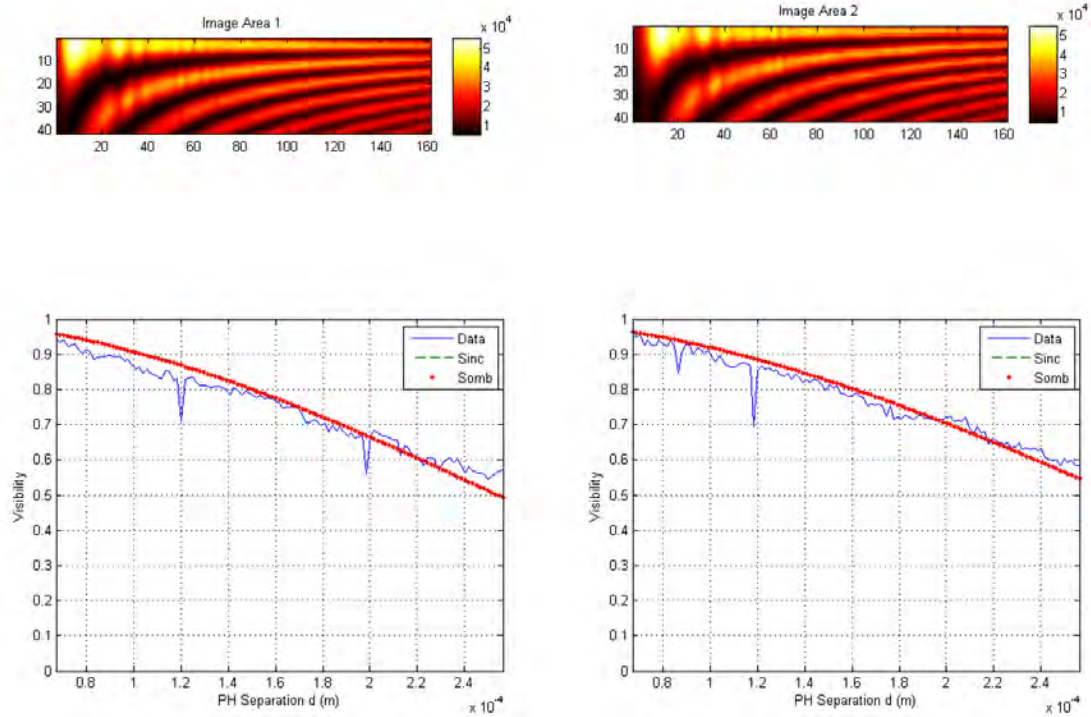


Figure 22: Results from the fit routine for the 0.5mm circular aperture ( $C_1$ ) and blocking the central area of the  $x$  aperture ( $S_3$ ). The first image area and its corresponding visibility fit (left). The second image area and its corresponding visibility fit (right). For this particular iteration, only a portion of the fringe pattern in the  $y_0$  range is selected to avoid temporal coherence effects. The red line corresponds to fitting a sombrero function to the visibility curve while the green line is a sinc function fit. The green line agrees with sombrero fit within ten percent so it is difficult to detect in the graph. The blue line resembles the data used in the fit routine.

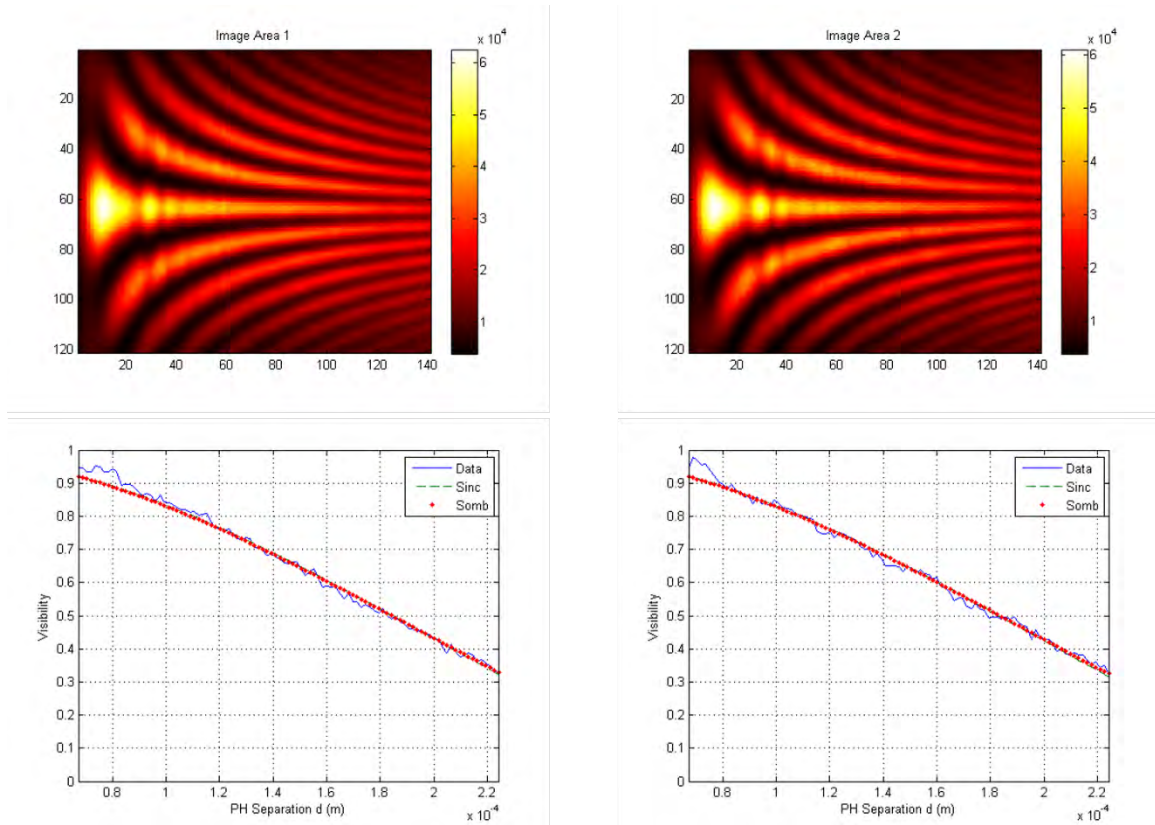


Figure 23: Image area selected on fringe pattern corresponding with the 1.5mm aperture ( $C_3$ ) and blocking the central area of the  $x$  aperture ( $S_3$ ) (left). Quadrant 2 image of the area scanned for the fit routine (right), where the quadrant is reflected about the  $y$ -axis before scanned. The red line corresponds to fitting a sombrero function to the visibility curve while the green line is a sinc function fit. The green line agrees with sombrero fit within ten percent so it is difficult to detect in the graph. The blue line resembles the data used in the fit routine.

Results of the fit routine are shown in Table 5. For 0.5mm source diameters ( $C_1$ ), the fit routine produces larger diameter estimates (positive error). For 1.0mm ( $C_1$ ) and 1.5mm ( $C_3$ ) circular apertures, the fit produces smaller diameter estimates (negative error). The difference between actual source diameters and the calculated source

diameters from the fit routine are larger for sinc fits compared to sombrero fits.

Interestingly, the 10 $\mu$ m slit with no block ( $S_2$ ) and the 12 $\mu$ m slit with no block ( $S_4$ ) yield the same fit value for the 1.0mm diameter source ( $C_2$ ). Having a center section of the x-aperture blocked, ( $S_1$ ) and ( $S_3$ ), seems to improve results.

Source (mm)	Diameter	Slit ( $\mu$ m)	Width	SINC fit (mm) (error)	SOMB fit (mm) (error)	X- Aperture Center
0.5 ( $C_1$ )		12 ( $S_1$ )		0.63 (+0.13)	0.73 (+0.23)	BLOCK
0.5 ( $C_1$ )		16 ( $S_3$ )		0.81 (+0.31)	0.94 (+0.44)	
1.0 ( $C_2$ )		12 ( $S_1$ )		0.75 (-0.25)	0.87 (-0.13)	
1.0 ( $C_2$ )		16 ( $S_3$ )		0.82 (-0.18)	0.95 (-0.15)	
1.5 ( $C_3$ )		12 ( $S_1$ )		1.07 (-0.43)	1.26 (-0.24)	
1.5 ( $C_3$ )		16 ( $S_3$ )		1.20 (-0.30)	1.40 (-0.10)	
0.5 ( $C_1$ )		14 ( $S_2$ )		N/A	N/A	NO BLOCK
0.5 ( $C_1$ )		14.5 ( $S_4$ )		0.609 (+0.11)	0.706 (+0.204)	
1.0 ( $C_2$ )		14 ( $S_2$ )		0.84 (-0.16)	0.98 (-0.02)	
1.0 ( $C_2$ )		14.5 ( $S_4$ )		0.84 (-0.16)	0.98 (-0.02)	
1.5 ( $C_3$ )		14 ( $S_2$ )		0.965 (-0.535)	1.45 (-0.05)	
1.5 ( $C_3$ )		14.5 ( $S_4$ )		1.09 (-0.41)	1.27 (-0.23)	

### *Sources of Error*

Four sources of error are identified in the experiment that result from the fabrication of the x-apertures. Scanning electron microscope images in Figure 24 show that the slit widths are not exactly 10 $\mu\text{m}$  and 12 $\mu\text{m}$  which is the first source of error. There are small variations along the length of the slits, and the slit average widths are to be 14.3 $\mu\text{m}$  (10 $\mu\text{m}$  design) and 15.9 $\mu\text{m}$  (12 $\mu\text{m}$  design).

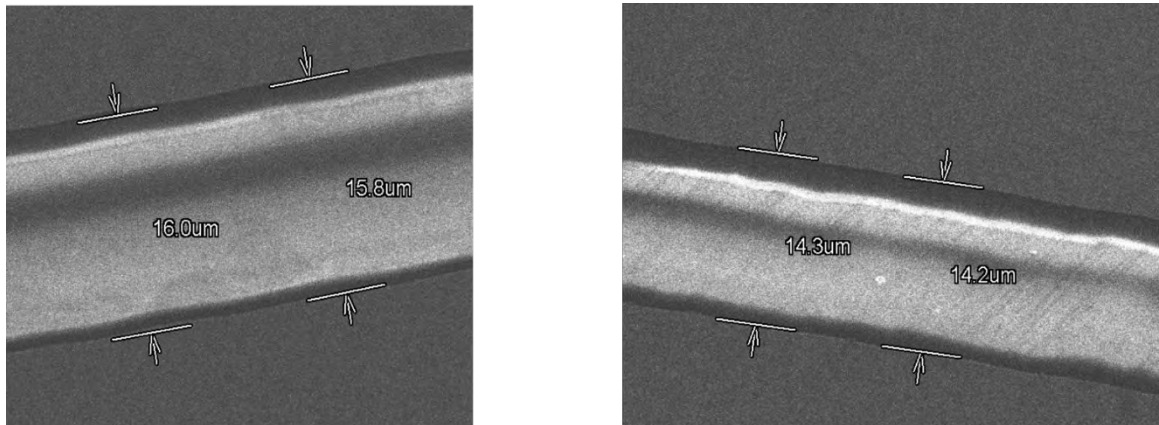


*Figure 24: SEM images of the 12 micron slit width x-aperture (left) and the 10 micron slit width aperture (right).*

The second source of error is the fabricated value of  $\theta_{\text{ap}}$ . The SEM images of the 10 $\mu\text{m}$  and 12 $\mu\text{m}$  x-aperture with no block ( $S_2$  and  $S_4$ ) have measured  $\theta_{\text{ap}}$  values of 21.96 $^\circ$  and 21.25 $^\circ$ , for the 10 $\mu\text{m}$  and 12 $\mu\text{m}$  designs, respectively (see Figure 25 and Figure 26). The use of the expression for the tangent

function and a simple radian to degrees conversion determines the angle measure given a triangle approximation between the slits.

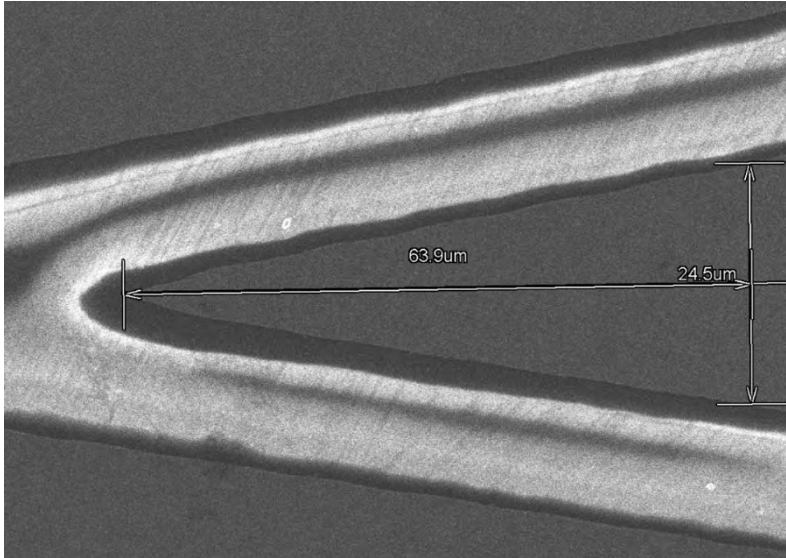


Figure 25: SEM image of the 10 micron slit width x-aperture ( $S_2$ ).

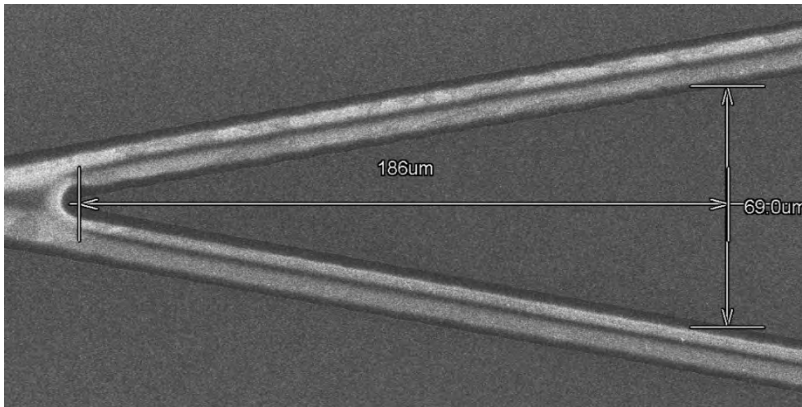
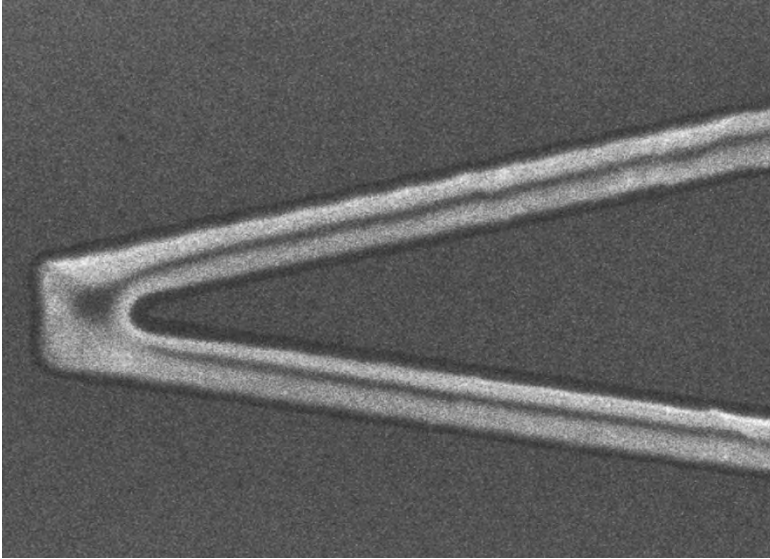


Figure 26: SEM image of the 12 micron slit width x-aperture ( $S_4$ ).

The third source of error is a physical connection between both slits in the fabrication of the x-apertures with a blocked center section ( $S_1$  and  $S_3$ ). This vertical segment is the leading suspect to the aforementioned spurious vertical diffraction lines

seen in multiple interferograms. The SEM image in Figure 27 displays the appearance of the vertical segment connecting the two slits.



*Figure 27: The SEM image of a vertical segment connecting the two slits near the center of the "x", for  $S_1$ .*

The fourth source of error could be chromatic aberration due to the dispersion in the glass substrate.

The next chapter summarizes the experimental results and discusses future work.



## CHAPTER 6: CONCLUSIONS

The spatial coherence of a 370nm UV LED source is measured using a single interferogram generated by an x-aperture interferometer. A simulation using OptiScan (Matlab package) of the experiment is performed. The experimental setup includes the source, circular aperture placed immediately in front of the source, the x-aperture and a camera. The camera and x-aperture are 1m away from the source- circular aperture pair. Recorded interferograms are in the form of a family of hyperbolae in each quadrant on a 2D observation plane. From the interferogram, the visibility is measured as a function of position and then a fit to an equation to determine an estimate of source diameter. Results for the simulation fit for a slit width of  $10\mu\text{m}$  ( $S_2$ ) and an actual source diameter of  $1.5\text{mm}$  ( $C_3$ ) yield an estimated  $1.40\text{mm}$  source diameter. The experimental data for the  $12\mu\text{m}$  slit width ( $S_3$ ) for a source diameter of  $1.5\text{mm}$  ( $C_3$ ) yield an estimated  $1.40\text{mm}$  source size. The worst fit result is for the  $0.5\text{mm}$  source size ( $C_1$ ), with the  $16\mu\text{m}$  ( $S_3$ ) slit width resulting in an estimated size of  $0.94\text{mm}$  diameter with the sombrero fit and  $0.84\text{mm}$  diameter for the sinc fit.

A key difference between the experiment and simulation occurs due to the fabrication of the x-apertures. The slit width simulated (10 and 12 microns) is different from the actual slit widths fabricated (14 and 16 microns). The significant increase in

width of the slits spreads the diffracted pattern at the observation plane and ultimately changes the fringe modulation. Another source of error arises from the fabrication of the blocked apertures, ( $S_1$ ) and ( $S_3$ ). Instead of the slits at angle completely disconnected from one another, the slits are bridged together near the center of the aperture. This bridging may explain the spurious diffraction lines seen at higher spatial frequencies, which changes maxima in intensity and the visibility. The third discrepancy is in the calculation of the angle between the slits. Instead of  $\theta_{ap} = 20^\circ$ ,  $\theta_{ap} = 21.96^\circ$  and  $\theta_{ap} = 21.25^\circ$  for  $S_2$  and  $S_4$ , respectively. Since  $d_{ph}$  is directly related to  $\theta_{ap}$ , the visibility is also altered, therefore manipulating experimental results. Finally, the temporal effects from the source wash out the visibility of the fringes affecting correct calculation.

There are a few changes that can be made to the experiment that could improve results. First, the bridge that connects the slits in ( $S_1$ ) and ( $S_3$ ) can be removed, in order to free the recorded pattern of spurious diffraction lines altering the visibility. Extending the slits beyond 2mm could achieve better results due to the larger range of pinhole spacings. It would also be more accurate to achieve a slit width closer to the ones simulated.

Future work includes fabricating more apertures and modification to the fit routine. For sources that are not symmetrical, adding in x-apertures in series at different angles would measure spatial coherence of different source points measured across the irregularly shaped source geometry. The reduction in visibility caused by the broad temporal power spectrum should also be factored into the calculation, since it has a dramatic effect on experimental results. One way to achieve this consideration may be to

define a function (one-to-one mapping) of the behavior of the temporal coherence as fringes transverse the  $y_0$  axis and subtract those effects from the calculation.

## REFERENCES

- [1] Milster, T. D. (2015). Laser Light Engineering.
- [2] Hooke, Robert “Robert Hooke’s Critique of Newton’s Theory of Light and Colors”. Thomas Birch, The History of the Royal Society, vol. 3 (London: 1757), pp. 10-15.
- [3] Huygens, Christiaan *Traité de la lumiere* (Leiden, Netherlands: Pieter van der Aa, 1690), Chapter 1.
- [4] Young, Thomas. A Course of Lectures on Natural Philosophy and the Mechanical Arts. Vol. 1. Lecture 39, “On the nature of light and colours”, p.457.
- [5] Fresnel, Augustin (1819). "Memoir on the Diffraction of Light". *The Wave Theory of Light – Memoirs by Huygens, Young and Fresnel*. American Book Company. pp. 79–145.
- [6] Wolf, Emil; Born, Max (1999). *Principles of optics: electromagnetic theory of propagation, interference and diffraction of light*. Cambridge: Cambridge University Press. p. 986.
- [7] SPIE (2014). "Philip Diamond plenary: The Square Kilometre Array: A Physics Machine for the 21st Century". SPIE Newsroom.
- [8] Hariharan, P. (2007). *Basics of Interferometry*, Second Edition. Elsevier.
- [9] Michelson, A. A., and Pease, F. G. (1921). *Astrophys. J.* 53, 249–259.
- [10] J.E. Trebes, K.A. Nugent, S Mrowka, R.A. London, T.W. Barbee, M.R. Carter, J.A. Koch, B.J. MacGowan, D.L. Matthews, L.B. Da Silva, G.F. Stone and M.D. Feit (1992). *Measurement of the Spatial Coherence of a Soft X-ray Laser*. *Physical Review Letters* Vol. 68, 5.
- [11] Yobani Mejia, A. I. (2007). *Measuring Spatial Coherence by Using a Mask with Multiple Apertures*. *Optical Communications* 273, 428-434.

[12] Dalip Singh Mehta, K. S. (2010). Coherence Characteristics of Light Emitting Diodes. Journal of Luminescence 130, 96-102.

[13] Tenio Popmintchev, Ming-Chang Chen, Dimitar Popmintchev, Paul Arpin, Susannah Brown, Skirmantas Alisauskas, Giedrius Andriukaitis, Tadas Balciunas, Oliver D. Mucke, Audrius Pugzlys, Andrius Baltuska, Bonggu Shim, Samuel E. Schrauth, Alexander Gaeta, Carlos Hernandez-Garcia, Luis Plaja, Andreas Becker, Agnieszka Jaron-Becker, Margaret M. Murnane, Henry C. Kapteyn (2012). Bright Coherent Ultrahigh Harmonics in the keV X-ray Regime from Mid-Infrared Femtosecond Lasers. Science AAAS 336, 1287-1291.

[14] J.J. A. Lin, D. Paterson, A.G. Peele, P.J. McMahon, C.T. Chantler, K.A. Nugent, B. Lai, N. Moldovan, Z. Cai, D.C. Marcini and I. McNulty (2003). Measurement of the Spatial Coherence Function of Undulator Radiation using a Phase Mask. Physical Review Letters 90, 7.

[15] Randy A. Bartels, Ariel Paul, Hans Green, Henry C. Kapteyn, Margaret M. Murnane, Sterling Backus, Ivan P. Christov, Yanwei Liu, David Attwood, Chris Jacobsen (2002). Generation of Spatially Coherent Light at Extreme Ultraviolet Wavelengths. ScienceMag Vol. 297.

[16] Maskless Lithography Tool. Milster Group 2016. University of Arizona. Department of Optical Sciences.

\* Derek S. Keyes, T. S.-S.-H. (2015). Optomechanical design and tolerance of a microscope objective at 121.6 nm. Proceedings of SPIE Vol. 9575.

\*Duarte F. J. (2007). Coherent electrically excited organic semiconductors: Visibility of interferograms and emission linewidth". Optics Letters Vol 32. No. 4 February 15, 2007.

\* Not specifically cited in document.

## Appendix A

Modeling Fit Routine:

```
%parameters
fid          = 100;
Xtheta      = 83;
z_src       = 1;
LAMBDA      = 365e-9;
```

```

%process mat file
%S      = load('fldslmmgrid9_70deg.mat');
%S      = load('fldslmmgrid9_70deg_5mm_z0.mat');
S      = load('Itotal_365LEDspectrum071415A.mat');
col_vec = S.sysxvec;
x_vec   = S.sysyvec;
Nsamps  = length(col_vec);
Ixt     = S.Itotal;

%allowcate data vector
contrast_vec = [];
l_vec       = [];

for kk = 300:301; %length(col_vec)

    y_vec = Ixt(:,kk);
    %disp(['kk = ' num2str(kk)])

    %expand data with interpolation
    N_interp_pixels = 8000;
    x_vec_exp       =
linspace(min(x_vec),max(x_vec),N_interp_pixels);
    y_vec_exp       = interp1(x_vec,y_vec,x_vec_exp,'spline');
    yavg_exp        = sum(y_vec_exp)/length(y_vec_exp);
    y_vec_exp       = y_vec_exp - yavg_exp;

    Npixels        = length(y_vec_exp);

    %find zero crossings
    transition_vec =
find(abs(diff(sign(y_vec_exp)))>0);%sort([indx_pos(pos_transition)
indx_neg(neg_transition)]);

    %Find peaks
    x_vec_exp_pos_peaks = [];
    y_vec_exp_pos_peaks = [];
    x_vec_exp_neg_peaks = [];
    y_vec_exp_neg_peaks = [];
    ii = 0;
    if length(transition_vec)>=2
        peak_flag = 1;
        while peak_flag
            %first check leading values for pos/neg peak
            if y_vec_exp(1) > 0 && ii == 0 %positive initial value
                temprange = 1:transition_vec(1);
                if max(y_vec_exp(temprange)) > y_vec_exp(1)+eps
%condition for peak in first segment
                    segment_indx = temprange;
                    pos_peak_flag = 1;

```

```

else          %no peak detected
    segment_indx = [];
end
ii = ii+1;
elseif y_vec_exp(1) < 0 && ii == 0 %negative initial value
    temprange = 1:transition_vec(1);
    if min(y_vec_exp(temprange)) < y_vec_exp(1)-eps
%condition for valley in first segment
        segment_indx = temprange;
        pos_peak_flag = 0;
    else          %no peak detected
        segment_indx = [];
    end
    ii = ii+1;
elseif (ii+1) <= length(transition_vec) &&
y_vec_exp(transition_vec(ii)+1) > 0 %positive full peak
    segment_indx =
transition_vec(ii):transition_vec(ii+1);
    pos_peak_flag = 1;
    ii = ii+1;
elseif (ii+1) <= length(transition_vec) &&
y_vec_exp(transition_vec(ii)+1) < 0 %negative full peak
    segment_indx =
transition_vec(ii):transition_vec(ii+1);
    pos_peak_flag = 0;
    ii = ii+1;
elseif ii == length(transition_vec) &&
y_vec_exp(transition_vec(ii)+1) > 0 %pos final section
    temprange = transition_vec(ii):length(y_vec_exp);
    if max(y_vec_exp(temprange)) > y_vec_exp(end)
%condition for peak in last segment
        segment_indx = temprange;
        pos_peak_flag = 1;
    else          %no peak detected
        segment_indx = [];
    end
    peak_flag = 0;
elseif ii == length(transition_vec) &&
y_vec_exp(transition_vec(ii)+1) < 0 %neg final section
    temprange = transition_vec(ii):length(y_vec_exp);
    if min(y_vec_exp(temprange)) < y_vec_exp(end)
%condition for valley in last segment
        segment_indx = temprange;
        pos_peak_flag = 0;
    else          %no peak detected
        segment_indx = [];
    end
    peak_flag = 0;
else
    peak_flag = 0;
end

```

```

        segment_indx    = [];
    end

    if ~isempty(segment_indx)
        if pos_peak_flag
            x_segment      = x_vec_exp(segment_indx) ;
            y_segment      = y_vec_exp(segment_indx) ;
            x_vec_exp_pos_peaks = [x_vec_exp_pos_peaks
x_segment(find(max(y_segment)==y_segment))];
            y_vec_exp_pos_peaks = [y_vec_exp_pos_peaks
max(y_segment)];
        else %negative peak
            x_segment      = x_vec_exp(segment_indx) ;
            y_segment      = y_vec_exp(segment_indx) ;
            x_vec_exp_neg_peaks = [x_vec_exp_neg_peaks
x_segment(find(min(y_segment)==y_segment))];
            y_vec_exp_neg_peaks = [y_vec_exp_neg_peaks
min(y_segment)];
        end
    end

    end

    figure(fid+1);plot(x_vec_exp,y_vec_exp
+yavg_exp,x_vec_exp_pos_peaks,y_vec_exp_pos_peaks+yavg_exp,'o' ...
,x_vec_exp_neg_peaks,y_vec_exp_neg_peaks+yavg_exp,'+');grid
axis([0 max(x_vec_exp) 0 max(Ixt(:))])
title(['Peak Locations: column ' num2str(kk)])
xlabel('Position (mm)')
ylabel('Irradiance')
pause(0.1)
if length(y_vec_exp_pos_peaks)>length(y_vec_exp_neg_peaks)
    y_vec_exp_pos_peaks      =
y_vec_exp_pos_peaks(1:length(y_vec_exp_neg_peaks));
elseif length(y_vec_exp_pos_peaks)<length(y_vec_exp_neg_peaks)
    y_vec_exp_neg_peaks      =
y_vec_exp_neg_peaks(1:length(y_vec_exp_pos_peaks));
end
    contrast_peaks          = (y_vec_exp_pos_peaks -
y_vec_exp_neg_peaks)./(y_vec_exp_pos_peaks + y_vec_exp_neg_peaks +
2*yavg_exp);
    contrast_vec            = [contrast_vec
sum(contrast_peaks)/length(contrast_peaks)];
    l_vec                   = [l_vec col_vec(kk)];
    if length(l_vec)>=2
        figure(fid+2);plot(l_vec,contrast_vec);axis([min(l_vec)
max(l_vec) 0 1]);grid
        xlabel('Distance along measuremetn axis (m)')
        ylabel('Visibility')
        grid
    end
end

```



```

        end

    end

%fit sinc and somb to data
d_vec      = 2*l_vec*tand(90-Xtheta);
myerror_sinc = @(D_src)
sqrt(sum((abs(sinc(d_vec/z_src/LAMBDA*D_src))-contrast_vec).^2));
myerror_somb = @(D_src)
sqrt(sum((abs(somb(d_vec/z_src/LAMBDA*D_src))-contrast_vec).^2));
D_sinc      = fminsearch(myerror_sinc, 1e-3);
D_somb      = fminsearch(myerror_somb, 1e-3);
disp(['Data fit to sinc function shows diameter = ' num2str(D_sinc)])
disp(['Data fit to somb function shows diameter = ' num2str(D_somb)])

%graph contrast vs d and show sinc and somb
figure(fid+3)
plot(d_vec,contrast_vec,'-',d_vec,sinc(d_vec/z_src/LAMBDA*D_sinc),'--
',d_vec,somb(d_vec/z_src/LAMBDA*D_somb),'.' )
axis([min(d_vec) max(d_vec) 0 1]);
grid
legend('Data','Sinc','Somb')
xlabel('PH Separation d (m)')
ylabel('Visibility')

```

### Experimental Fit Routine:

```

%process_contrast_vs_OPD_061815_Brush_andNoBrush.m

%parameters
fid      = 100;
Xtheta   = 80;
z_src    = 1;
LAMBDA   = 370e-9;

%process mat file
%S       = load('flds1mmgrid9_70deg.mat');
%S       = load('flds1mmgrid9_70deg_5mm_z0.mat');
fname2 = '08082016_1p5mmap_noblock_10um_1m.tif';
X2 = imread(fname2,'tif'); %omit X2 = rgb2gray(imread(fname2,'tif'));
figure(10);imagesc(X2);
colormap(hot);
axis image;
colorbar
%set background image area
row_vec_bknd = 1:200;
col_vec_bknd = 1:200;
%image 1 area
row_vec1     = 1780:1860;

```

```

col_vec1    = 1860:1990;
%image 2 area
row_vec2    = 1780:1860;
col_vec2    =1660:1790;           %col_vec2    = (1099-length(col_vec1)+1):1099;

%define working images
Xsmall1 = double(X2(row_vec1,col_vec1));
figure(5);imagesc(Xsmall1);colormap(hot);axis image;colorbar
title('Image Area 1')
Xsmall2 = fliplr(double(X2(row_vec2,col_vec2)));
figure(6);imagesc(Xsmall2);colormap(hot);axis image;colorbar
title('Image Area 2')
col_vec    = 0:(length(col_vec1)-1);

%calculate background
Xbknd     = double(X2(row_vec_bknd,col_vec_bknd));
[nr,nc]   = size(Xbknd);
avgbknd   = sum(Xbknd(:))/nr/nc;
% S       = load('08082016_0p5mmap_block_12um_1m.tif');
% col_vec = S.sysxvec;
% x_vec   = S.sysyvec;
% Nsamps  = length(col_vec);
% Ixt     = S.Itotal;
Nsamps    = length(col_vec1);
x_vec     = 4.54e-6*(0:(length(row_vec1)-1));
%Ixt     = X2small-min(X2small(:));
[nr,nc]   = size(Xsmall1);
Ixtmat    = zeros(nr,nc,2);
Ixtmat(:,1) = Xsmall1-5600;%avgbknd;
Ixtmat(:,2) = Xsmall2-5600;%avgbknd;
% Ixt     = X2small;

for mm = 1:2

    Ixt    = squeeze(Ixtmat(:,:,mm));

%allocate data vector
contrast_vec = [];
l_vec       = [];

for kk = 43:length(col_vec1); %length(col_vec)

    y_vec   = Ixt(:,kk);
    %disp(['kk = ' num2str(kk)])

%expand data with interpolation
N_interp_pixels = 8000;

```

```

x_vec_exp      = linspace(min(x_vec),max(x_vec),N_interp_pixels);
y_vec_exp      = interp1(x_vec,y_vec,x_vec_exp,'spline');
yavg_exp       = sum(y_vec_exp)/length(y_vec_exp);
y_vec_exp      = y_vec_exp - yavg_exp;

Npixels        = length(y_vec_exp);

%find zero crossings
transition_vec  = find(abs(diff(sign(y_vec_exp)))>0);%sort([indx_pos(pos_transition)
indx_neg(neg_transition)]);

%Find peaks
x_vec_exp_pos_peaks = [];
y_vec_exp_pos_peaks = [];
x_vec_exp_neg_peaks = [];
y_vec_exp_neg_peaks = [];
ii              = 0;
if length(transition_vec)>=2
    peak_flag    = 1;
    while peak_flag
        %first check leading values for pos/neg peak
        if y_vec_exp(1) > 0 && ii == 0 %positive initial value
            temprange    = 1:transition_vec(1);
            if max(y_vec_exp(temprange)) > y_vec_exp(1)+eps %condition for peak in first segment
                segment_indx = temprange;
                pos_peak_flag = 1;
            else %no peak detected
                segment_indx = [];
            end
            ii = ii+1;
        elseif y_vec_exp(1) < 0 && ii == 0 %negative initial value
            temprange    = 1:transition_vec(1);
            if min(y_vec_exp(temprange)) < y_vec_exp(1)-eps %condition for valley in first segment
                segment_indx = temprange;
                pos_peak_flag = 0;
            else %no peak detected
                segment_indx = [];
            end
            ii = ii+1;
        elseif (ii+1) <= length(transition_vec) && y_vec_exp(transition_vec(ii)+1) > 0 %positive full peak
            segment_indx = transition_vec(ii):transition_vec(ii+1);
            pos_peak_flag = 1;
            ii = ii+1;
        elseif (ii+1) <= length(transition_vec) && y_vec_exp(transition_vec(ii)+1) < 0 %negative full peak
            segment_indx = transition_vec(ii):transition_vec(ii+1);
            pos_peak_flag = 0;
            ii = ii+1;
        elseif ii == length(transition_vec) && y_vec_exp(transition_vec(ii)+1) > 0 %pos final section
            temprange    = transition_vec(ii):length(y_vec_exp);
            if max(y_vec_exp(temprange)) > y_vec_exp(end) %condition for peak in last segment

```

```

        segment_indx = temprange;
        pos_peak_flag = 1;
    else %no peak detected
        segment_indx = [];
    end
    peak_flag = 0;
elseif ii == length(transition_vec) && y_vec_exp(transition_vec(ii)+1) < 0 %neg final section
    temprange = transition_vec(ii):length(y_vec_exp);
    if min(y_vec_exp(temprange)) < y_vec_exp(end) %condition for valley in last segment
        segment_indx = temprange;
        pos_peak_flag = 0;
    else %no peak detected
        segment_indx = [];
    end
    peak_flag = 0;
else
    peak_flag = 0;
    segment_indx = [];
end

if ~isempty(segment_indx)
    if pos_peak_flag
        x_segment = x_vec_exp(segment_indx);
        y_segment = y_vec_exp(segment_indx);
        x_vec_exp_pos_peaks = [x_vec_exp_pos_peaks
x_segment(find(max(y_segment)==y_segment))];
        y_vec_exp_pos_peaks = [y_vec_exp_pos_peaks max(y_segment)];
    else %negative peak
        x_segment = x_vec_exp(segment_indx);
        y_segment = y_vec_exp(segment_indx);
        x_vec_exp_neg_peaks = [x_vec_exp_neg_peaks
x_segment(find(min(y_segment)==y_segment))];
        y_vec_exp_neg_peaks = [y_vec_exp_neg_peaks min(y_segment)];
    end
end

end

figure(fid+1+10*(mm-1));plot(x_vec_exp,y_vec_exp
+yavg_exp,x_vec_exp_pos_peaks,y_vec_exp_pos_peaks+yavg_exp,'o' ...
,x_vec_exp_neg_peaks,y_vec_exp_neg_peaks+yavg_exp,'+');grid
axis([0 max(x_vec_exp) 0 max(Ixt(:))])
title(['Peak Locations: column ' num2str(kk)])
xlabel('Position (m)')
ylabel('Irradiance')
pause(0.1)
if length(y_vec_exp_pos_peaks)>length(y_vec_exp_neg_peaks)
    y_vec_exp_pos_peaks = y_vec_exp_pos_peaks(1:length(y_vec_exp_neg_peaks));
elseif length(y_vec_exp_pos_peaks)<length(y_vec_exp_neg_peaks)
    y_vec_exp_neg_peaks = y_vec_exp_neg_peaks(1:length(y_vec_exp_pos_peaks));
end
end

```

```

        contrast_peaks = (y_vec_exp_pos_peaks - y_vec_exp_neg_peaks)./(y_vec_exp_pos_peaks +
y_vec_exp_neg_peaks + 2*yavg_exp);
        contrast_vec = [contrast_vec sum(contrast_peaks)/length(contrast_peaks)];
        l_vec = [l_vec col_vec(kk)];
        if length(l_vec)>=2
            figure(fid+2);plot(l_vec,contrast_vec);axis([min(l_vec) max(l_vec) 0 1]);grid
            xlabel('Distance along measurement axis (m)')
            ylabel('Visibility')
            grid
        end
    end
end

%fit sinc and somb to data
d_vec = 4.54e-6* 2*l_vec*tand(90-Xtheta);
myerror_sinc = @(D_src) sqrt(sum((abs(sinc(d_vec/z_src/LAMBDA*D_src))-contrast_vec).^2));
myerror_somb = @(D_src) sqrt(sum((abs(somb(d_vec/z_src/LAMBDA*D_src))-contrast_vec).^2));
D_sinc = fminsearch(myerror_sinc, 1e-3);
D_somb = fminsearch(myerror_somb, 1e-3);
disp(['Data fit to sinc function shows diameter = ' num2str(D_sinc)])
disp(['Residual RMS error for sinc : ' num2str(myerror_sinc(D_sinc)/length(contrast_vec))])
disp(['Data fit to somb function shows diameter = ' num2str(D_somb)])
disp(['Residual RMS error for somb : ' num2str(myerror_somb(D_somb)/length(contrast_vec))])

%graph contrast vs d and show sinc and somb
figure(fid+3+10*(mm-1))
plot(d_vec,contrast_vec,'-',d_vec,sinc(d_vec/z_src/LAMBDA*D_sinc),'--
',d_vec,somb(d_vec/z_src/LAMBDA*D_somb),'-')
axis([min(d_vec) max(d_vec) 0 1]);
grid
legend('Data','Sinc','Somb')
xlabel('PH Separation d (m)')
ylabel('Visibility')

end

```

## Appendix B

Source Specifications:

ENGIN 365nm UV LED  
 Model #: LZ4-00U600  
 Footprint: 7.0mm x 7.0mm  
 Peak Wavelength: 365nm  
 Bandwidth: 359nm – 371nm

## **Appendix C**

### Camera Specifications:

Sony Kingfisher CCD (SONY ICX694)

Sensor: 1" Scientific CCD

Active Pixel Resolution: 2750 x 2200

Pixel Size: 4.54 $\mu$ m x 4.54 $\mu$ m

Active Area: 12.49mm (H) x 9.99mm (V)

Spectral Response: 310nm – 1100nm